ICAL
ETY

MEMOIRS

OF THE

COLLEGE OF SCIENCE

KYOTO IMPERIAL UNIVERSITY

SERIES A

VOL. XXI, NO. 6

NOVEMBER 1938

KYOTO

On the Balmer Emission of the Planetary Nebulae

By **Shôtarô Miyamoto**

(Received September 6, 1938)

Introduction

§ 1. Since 1927 when H. Zanstra[1] put forward the hypothesis of recombination mechanism to explain the phenomena of the Balmer Emission in the planetary nebulae, this theory has been discussed from different aspects and applied on various problems of astrophysics. One of the most important investigations is that of G. G. Cillié[2], who has attempted to account for the Balmer decrement, assuming the complete transparency of the nebula with respect to the subordinate lines. His theory seemed at first not to be well supported by the observations, so far as the observed decrement was often steeper than the theoretical prediction; but this discrepancy has mostly been removed by the introduction of a correction for the space reddening, as recently proposed by L. Berman[3].

So far, the observed hydrogen emissions have been approximately explained in terms of the recombination theory. Notwithstanding there seem to exist in such current treatments of the problem certain very essential defects from the theoretical point of view, which may be enumerated as follows:—

a) The theoretical decrement is rather insensitive to the variation of the electron temperature T_e, and fails to explain the observed dispersion in the decrement; for example, the intensity ratio of the first two Balmer emissions, H_α/H_β increases only from 2.7 to 2.8 as T_e increases from 5,000° to 10,000°, and even for $T_e=50{,}000°$ it barely attains to 3.0, while for the nebula N. G. C. 7027, observed decrement amounts to 3.9, and this seems not to correspond to any reasonable electron temperature.

b) As has been pointed out by Cillié[2], the continuous Balmer emission is in some cases much weaker than would be expected from

1. H. Zanstra, ZS. f. Astrophysik. **2** (1931)1, 329.
2. G. G. Cillié, M. N. **92** (1932) 820, **96** (1936) 771.
3. L. Berman, Ibid. **96** (1936) 890.

the theory; i. e. discrete Balmer emission appears too strong compared with it. Such a discrepancy seems to be untenable, as will easily be seen, if we remember the fundamental mechanism of the theory that the continuous part of the Balmer emission is emitted by the direct capture of free electrons to the second level, while its discrete lines are caused by the transitions of electrons from the higher levels, to which they were directly captured, or to which they had cascaded down from still higher ones, having had captured therein.

c) If the free electrons in the nebulae are assumed to have a velocity distribution obeying the Maxwellian law, we are able to predict the intensity distribution of the continuous Balmer emission, provided the probability for capture is given as a function of the velocity of the impinging electron. The theory predicts a monotonous diminution of the emission intensity beyond the Balmer limit λ 3647 Å for any value of T_e. Observation available to verify this fact is that of T. L. Page[1], which is on the whole in line with the theory except that it often shows a hump at about λ 3530 Å. This may mean that the distribution of the electron velocities in the nebula does not exactly obey the Maxwellian law; or that the analysis of the observed data does not result in this law. On the other hand, as will be seen later (§ 7), mutual collision between electrons occurs in the nebula, much more frequently than recombination and ionization; therefore we are forced against Page's observation to conclude that the collision effect must keep the Maxwellian distribution, smoothing out the tendencies of both the increasing high speed electrons and the decreasing slow ones, caused by the photoelectric ionization and by the recombination with protons respectively. In any case, we can, as Page first has done, roughly derive the electron temperature from the slope of the observed continuous emission; but the temperature obtained in such a way seems to be the lower, the steeper the Balmer decrement, in the sense contrary to that resulted from the theory.

d) The method of temperature estimation above mentioned gives[1] 700°–1,600° and 1,200°–4,000° for N. G. C. 7027 and 7662 respectively; these objects belong to a group of nebulae, characterized by intensive nebulium emission, taking the intensity of H_β as standard; 2,700°–4,500° and 2,200°–11,000° for N. G. C. 6572 and I. C. 4593 belonging to another group with less intensive nebulium emission. These estimates, although

1. T. L. Page, M. N. **96** (1936) 604.

they were unexpectedly low, have been accepted generally without any detailed discussion. But the result seems not to be so trivial. Indeed, it is well known that the nebulium emission is only explainable by the excitation due to the electron impact[1]; but even this effect may be inadequate to account for the emission mechanism because in such a low temperature gas, electrons, which have sufficient kinetic energy to excite the nebulium elements are too scanty. For example, a temperature of 4,000° or higher seems to be necessary for electrons to excite the chief nebulium lines $\lambda\lambda$ 4959 and 5007 of O_{III}. Incidentally it may be interesting to remark that the observed temperature seems lower, as the nebulium lines appear brighter. The circumstances above stated are rather to be interpreted as such that the appearance of higher energy radiations such as $\lambda\lambda$ 3726 and 3729 of O_{II}, and $\lambda\lambda$ 3869 and 3968 of Ne_{III} etc., suggests a considerable order of magnitude for T_e.

§ 2. The effect of self-reversal has often been suggested to explain the anomalies enumerated in the preceding paragraph[2]. The reason consists in the tendency of considerable accumulation of atoms in levels $2S$ and $2P$, in the former case on account of its metastability and in the latter on account of the denseness of the radiation of Lyman α,[3] to which the nebular matter is very opaque; this means that Cillié's assumption on the transparency of the nebula to the subordinate lines must be abandoned. But, as will be briefly discussed in §§ 24–26, from such a line of attack no straight solution of the problem seems to be obtained with any reasonable assumptions as to the nebular conditions. The problem, however, seems to be more naturally solved if we take into account the effect of collision.

In this paper a general theory will be formulated of the collisional excitation of the normal hydrogen atom by electron. In Chap. I, the emission mechanism of Balmer lines is treated generally, taking into account both the recombination and collision. For the practical application of the theory, it is necessary to know quantitatively the cross-sections for the inelastic collision inducing the excitation of the atom. For high speed collisions computations are rather simple, and fully discussed by many authors[4]; but the case immediately interesting for the nebular problem is that of the so-called slow collision, especially

1. I. S. Bowen. Ap. J. **67** (1928) 1.
2. V. Ambaruzumian. Pulkovo Circ. No. 6 (1935), M. N. **93** (1933) 50.
3. Cillié, *loc. cit.*
4. Cf. for instance, H. Bethe, Hb. d. Physik. Bd. XXIV/1. (1933) III.

so slow as to be just above the limit of excitation potential. In such a case, the mathematical expressions become so complicated that it is practically impossible to carry out numerical computations of them. In the last chapter of this paper, is a summarized method of approximate calculation together with results obtained. These results are used in the application of the theory on the nebulae (Chap. II and III), and it is shown that the very anomalies stated in § 1 can be explained. It is also found that a definite idea on the electron temperature of the nebulae is revealed.

I. General Theory

Ionization formula

§ 3. Degree of ionization in a hydrogen gas of temperature T_e, exposed to the diluted high temperature radiation is given by the well-known formula, in which two balancing processes have been considered : viz. photoelectric ionization and capture of free electrons. To include the collision effect, only a slight modification is required to the current formula.

Prior to our modified treatment, we may reproduce briefly, after S. Rosseland[1], the derivation of the current formula. Let N_1, N_c and N_e be the concentrations of hydrogen atoms in the normal, in the ionized state, and of free electrons respectively, neglecting all the intermediate states. For all transitions out of and into the given state, the conservation of energy is expressed by

$$N_1 a_{1c} = N_e N_c a_{c1},$$

where a_{1c} and a_{c1} are the transition probabilities due to the photoelectric ionization and recombination, multiplied by the energies associated therewith. Or, assuming $N_e = N_c$, viz. that the nebula is composed mainly of the hydrogen gas, we have

$$N_1 a_{1c} = N_e^2 a_{c1}. \tag{3.1}$$

In order to calculate a_{1c} and a_{c1}, we have to know the atomic absorption coefficient σ_ν in the ultraviolet region, and the probability of recombination. But it is sufficient to know one of them, since they are connected, as is well known, by the thermodynamical relations. Now in the nebula we have a field of the diluted temperature radiation, so that its density is

$$\frac{1}{\delta}\,\frac{8\pi h\nu^3}{c^3}\left(e^{\frac{h\nu}{kT_*}}-1\right)^{-1}$$

1. S. Rosseland, Theoretical Astrophysics. (1936) Chap. XII, § 116.

$$\delta=\frac{4r^2}{r_*^2}, \tag{3.2}$$

where r_*, r are the radius of the central star and of the nebulous shell, T_* the effective temperature of the nuclear star, and the other notations are as usual. On the other hand, we may safely assume that in the nebula, the velocity distribution of electrons is Maxwellian corresponding to a temperature Te generally different from that of the central star. Thus Rosseland has derived the following expressions, approximating σ_ν by the Kramers' formula : $\sigma_\nu \backsim \nu^{-3}$,

$$\left.\begin{aligned} a_{1c}&=\frac{1}{\delta}\,\frac{8\pi\sigma_1}{c^2}kT_*e^{-h\nu_1/kT_*}\\ a_{c1}&=\frac{8\pi\sigma_1 kTe}{\tilde{\omega}c^2 f_e}\\ \sigma_\nu&=\sigma_1\nu^{-3}\qquad \nu>\nu_1=\chi_1/h\\ \sigma_1&=\frac{16\varepsilon^2\nu_1^2}{3\sqrt{3}mc}\\ f_e&=2(2\pi mkTe)^{3/2}h^{-3} \end{aligned}\right\} \tag{3.3}$$

where χ_1 means the ionization potential of the hydrogen atom, ν_1 the frequency of Lyman limit, and $\tilde{\omega}$ the ratio of the weight of the ionized to that of the normal state. Hence it follows from (3.1), the required formula of ionization ;

$$\frac{Ne^2}{N_1}=\frac{1}{\delta}\,\frac{2\tilde{\omega}(2\pi mkT_*)^{3/2}}{h^3}e^{-h\nu_1/kT_*}\sqrt{\frac{Te}{T_*}}. \tag{3.4}$$

§ 4. To include the effect of collision in the formula, (3.1) must be replaced by

$$N_1a_{1c}+N_1N_e\gamma_{1c}=N_e^2a_{c1}, \tag{4.1}$$

where γ_{1c} is the term of collisional ionization[1], which is expressed by

$$N_e\gamma_{1c}=\int_{v_1}^{\infty}h\nu\cdot Q(v)v\cdot N_e(v)dv, \tag{4.2}$$

with v=velocity of colliding electron,

v_1=equivalent electron velocity of Lyman limit,

$N_e(v)dv$=concentration of electrons in interval $(v, v+dv)$ per cm^3,

$Q(v)$=effective area for ionization,

$h\nu$=energy of the expelled electron.

As to $h\nu$, it is admissible, to replace it by $h\nu_1$ in practice. If we put the mean value of $Q(v)$,

1. The converse process is neglected compared with $N_e^2a_{c1}$; it is, indeed, a three body collision of two electrons and a proton, so that its frequency may be very small compared with that of simple capture $N_e^2a_{c1}$, unless its probability is extremely large.

$$\bar{Q}\equiv\frac{\int_{v_1}^{\infty}h\nu Q(v)v N_e(v)dv}{h\bar{\nu}\int_{v_1}^{\infty}v N_e(v)dv}, \tag{4.3}$$

we get $$N_e\gamma_{1c}=h\nu_1\bar{Q}\int_{v_1}^{\infty}v N_e(v)dv\,;$$

or $$\gamma_{1c}=h\nu_1\bar{Q}\phi(T_e), \tag{4.4}$$

with $$\phi(T_e)\equiv\int_{v_1}^{\infty}v\frac{N_e(v)}{N_e}dv,$$

or, inserting Maxwell's expression in $N_e(v)$ and integrating,

$$\phi(T_e)=4\left(\frac{k}{2\pi m}\right)^{1/2}T_e^{1/2}\left(1+\frac{\chi_1}{kT_e}\right)e^{-\chi_1/kT_e}. \tag{4.5}$$

Now we are able to solve the equation (4.1):

$$\frac{N_e}{N_1}=\frac{1}{2}\left[\frac{\gamma_{1c}}{a_{c1}}+\sqrt{\left(\frac{\gamma_{1c}}{a_{c1}}\right)^2+\frac{4}{N_1}\left(\frac{a_{1c}}{a_{c1}}\right)}\right], \tag{4.6}$$

which becomes by (3.3) and (4.4),

$$\frac{N_e}{N_1}=\frac{1}{2}\left[\frac{h\nu_1\bar{Q}\phi(T_e)}{\frac{8\pi\sigma_1}{\tilde{\omega}c^2f_e}\cdot kT_e}+\sqrt{\left(\frac{h\nu_1\bar{Q}\phi(T_e)}{\frac{8\pi\sigma_1}{\tilde{\omega}c^2f_e}\cdot kT_e}\right)^2+\frac{4}{N_1}\cdot\frac{1}{\delta}\tilde{\omega}f_e\left(\frac{T_*}{T_e}\right)e^{-\frac{h\nu_1}{kT_*}}}\right]. \tag{4.7}$$

When the collisional effect is negligible, it of course degenerates into the ordinary form (3.4). On the contrary, when it dominates,

$$\frac{N_e}{N_1}=\frac{h\nu_1\bar{Q}\phi(T_e)}{\frac{8\pi\sigma_1}{\tilde{\omega}c^2f_e}\cdot kT_e}. \tag{4.8}$$

§ 5. To carry out numerically the computation of (4.7) or (4.8), we must know the values of $\bar{Q}$ and N_1.

First, as to the probabilities of collisional ionization, laborious calculations have been performed by H. S. W. Massey and C. B. O. Mohr[1]. At the series limit, it has a vanishing probability and rapidly increases with the velocity of colliding electron and attains a maximum of about πa_0^2, where a_0 means Bohr's radius of hydrogen. Generally speaking, $\bar{Q}$ in (4.3) depends on T_e, but for our purpose a good approximation is obtained, replacing $\bar{Q}$ by its mean value $\bar{Q}\fallingdotseq 0.2\pi a_0^2$.

Secondly, we assume, with Zanstra[2], that the ultraviolet radiation from the central star is almost completely absorbed by its enveloping hydrogen nebula. The atomic absorption coefficient beyond the Lyman

1. Mott and Massey, The Theory of Atomic Collisions. (1933) Chap. XI § 3.
2. Zanstra, *loc. cit.*

limit amounts to 0.54×10^{-17}, so that for the almost complete absorption, (optical depth unity say), there must be $1/(0.54 \times 10^{-17})$ normal atoms per square cm., which corresponds to $N_1 = 6$ for a nebular shell of thickness 2,000 A. U. at the distance 10,000 A. U. from the nucleus, as is the case in the typical nebula.

§ 6. Thus adopting the values $\bar{Q} = 0.2\,\pi a_0^2$ and $N_1 = 6$, we have carried out numerical computations, of which the results are reproduced in Table I.

Table I. Values of $\frac{N_e}{N_1} \times 10^{-2}$ ($N_1 = 6$, $\bar{Q} = 0.2\pi a_0^2$)

T_*	$\log \delta$	T_e 8,000	10,000	12,500	15,000	17,500	20,000	22,500	25,000	30,000	40,000
20,000	13	1.68	1.82	1.82	1.95	2.16	2.28				
	14	0.518	0.575	0.58	0.620	0.695	0.85				
	15	0.164	0.182	0.184	0.205	0.268	0.456				
	16	0.052	0.058	0.060	0.075	0.146	0.375				
30,000	13	8.2	8.6	9.1	9.6	10.0	10.4	11.0	11.8	14.2	
	14	2.58	2.74	2.89	3.04	3.20	3.40	3.82	4.49	7.00	
	15	0.815	0.865	0.915	0.965	1.05	1.21	1.59	2.36	5.40	
	16	0.258	0.274	0.290	0.313	0.378	0.550	1.01	1.92	5.20	
40,000	13	16.4	18.2	18.2	19.2	20.2	20.6	21.8	23.0	25.4	37.0
	14	5.18	5.75	5.75	6.1	6.40	6.65	7.20	7.85	10.2	23.4
	15	1.64	1.82	1.82	1.93	2.06	2.23	2.62	3.32	6.00	21.2
	16	0.515	0.575	0.580	0.625	0.695	0.850	1.25	2.09	5.29	20.9
50,000	13	25.8	27.4	28.8	30.0	31.4	32.4	33.9	35.4	38.8	50.6
	14	8.15	8.65	9.1	9.52	9.95	10.1	11.0	11.8	14.2	26.6
	15	2.58	2.74	2.88	3.02	3.19	3.40	3.82	4.50	7.00	21.6
	16	0.815	0.865	0.915	0.99	1.05	1.21	1.58	2.36	5.40	20.9
60,000	13	40.8	43.4	44.8	48.0	49.5	51.5	53.5	56.5	59.5	73.0
	14	12.9	13.7	14.1	15.0	15.7	16.3	17.1	18.2	20.8	32.6
	15	4.08	4.34	4.48	4.76	5.00	5.30	5.75	6.45	8.80	22.6
	16	1.29	1.37	1.42	1.54	1.62	1.80	2.18	2.89	5.60	21.0

The heavy lines in the table indicate the very limit, of which the right hand side corresponds to the domain where the ionization is effected by collision in a perceptible amount—say, half as much as photo-electrically, or more, and as the electron temperature T_e increases, after passing this line to the right, the degree of ionization increases rapidly and becomes much higher than that given by the current formula (3.4).

§ 7. A short note will be added here on a basal assumption of our theory. We have assumed that a local electron temperature T_e exists at each point within the nebula; or, in detail, that the electron velocities are distributed in a Maxwellian form, so that their states are represented by one parameter T_e, at least in a first approximation and that capturing processes take place under this condition. The Maxwellian distribution is in this case disturbed by two functions, viz. the capture and the photoelectric ionization, and conserved by the mutual collision of electrons (cf. § 1 c).

In order to be able to make use of the parameter T_e, the latter process must be proved to be much powerful than the former. This is, indeed, the case; for example, in the nebula of ionization degree 100, a rough estimate shows that the mutual collision occurs as frequently as once a day, while the ionization or capture once a year, or less. Thus the assumption on the existence of the local electron temperature seems to work out to self-consistent results[1, 2].

Cyclic Equations

§ 8. With Zanstra[3] and Cillié[4], we assume the following conditions in the nebula:

(i) Nebula is mainly composed of hydrogen gas.

(ii) The photoelectric ionization is succeeded by a capture of free electron; if the electron is captured in a higher state, it cascades down till to the lowest state. (But the reverse process can be omitted[5]).

(iii) Nebula is transparent to the subordinate lines.

(iv) Nebula is so opaque to Lyman radiation that these radiations, if created in it, are completely reabsorbed and split into a quantum of Balmer lines and that of L_α, before leaving the nebula.

§ 9. The equation of quanta is then[4],

$$N_n \sum_{r=2}^{n-1} A_{n,r} = G_n(T_e) + \sum_{r=1}^{\infty} N_{n+r} A_{n+r,n}. \qquad (n=3, 4, \ldots\ldots) \qquad (9.1)$$

N_n means the number of atoms in the n-th state per c.c., $A_{n,r}$ the

1. J. H. Jeans, Dynamical Theory of Gases, (1916) § 353.

2. It would be worth while to remark here, that any start from a non-Maxwellian distribution will lead one to self-contradiction, even if one takes into account the dissipation of the kinetic energy induced by the nebulium excitation.

3. Zanstra, *loc. cit.*

4. Cillié, *loc. cit.*

5. It follows from the condition (iii).

transition probability from the n-th to the r-th state. By the processes of recombination and collision, the atom is brought to the n-th state; let the number of such atoms be $G_n(Te)$ per c.c., per sec. The number of atoms which come down to this state from the higher ones is represented by the second term in the right side of the equation. Thus the equation balances the number of quanta arriving at this state against that of leaving there by the downward transitions[1], the complete opaque of the nebula to the Lyman radiation being introduced in summing up $A_{n,r}$ from $r=2$ to $n-1$.

For our purpose, or to evaluate the ratio $H\alpha : H\beta$, exhaustive calculation is unnecessary, and hence we shall neglect states higher than the fifth. Then (9.1) becomes

$$N_n \sum_{r=2}^{n-1} A_{n,r} = G_n(Te) + \sum_{r=1}^{n+r=5} N_{n+r} A_{n+r,n} . \qquad (n=3, 4, 5)$$

This is a set of simultaneous equations with respect to N's, of which the solution is

$$\begin{aligned} 10^8 N_3 &= 2.28\ G_3 + 1.189\ G_4 + 1.106\ G_5 \\ 10^8 N_4 &= \qquad 5.84\ \ G_4 + 2.12\ \ G_5, \end{aligned} \qquad (9.2)$$

where numerical values of the transition probabilities have been taken from the work of D. H. Menzel and C. L. Pekeries[2].

§ 10. It is now convenient to give separate expressions in G-terms both for the capture and collision. To see clearly their dependency on the electron density, we put

$$\begin{aligned} G_n(Te) &= N_e^2 \mathfrak{C}_n(Te) + N_e N_1 \mathfrak{D}_n(Te) \\ \text{or} \qquad &= N_e N_1 \left[\frac{N_e}{N_1} \mathfrak{C}_n(Te) + \mathfrak{D}_n(Te) \right]. \end{aligned} \qquad (10.1)$$

(i) The part of capture $\mathfrak{C}_n(Te)$ is nothing but that of Cillié[3], which he derived from the J. A. Gaunt's absorption coefficient[4]:

$$\begin{aligned} \mathfrak{C}_n(Te) &= \frac{2^9 \pi^5}{(6\pi)^{3/2}} \frac{\epsilon^{10}}{m^2 c^3 h^3} \left(\frac{m}{k} \right)^{3/2} \cdot \frac{1}{Te^{3/2}} \frac{1}{n^3} e^{\chi_n / kTe} [-E_i(-\chi_n / kTe)] \\ &= 3.22 \times 10^{-6} \cdot M_n(Te). \end{aligned} \qquad (10.2)$$

(ii) The collisional term is

$$\mathfrak{D}_n(Te) = \int_{v_n}^{\infty} Q_n(v) \frac{v \cdot N_e(v)}{N_e} dv,$$

---

1. The photoelectric ionization from states other than the normal one are negligible, owing to the smallness of the population therein. Similarly, the same holds as for the excitation or de-excitation by collision.
2. D. H. Menzel and C. L. Pekeries, M. N. **96** (1936) 77.
3. Cillié, *loc. cit.*
4. J. A. Gaunt, Phil. Trans. A. **229** (1929) 200.

where v_n=electron velocity equivalent to the excitation potential of the n-th state, $\chi_1-\chi_n$.

$N_e(v)dv$=concentration of electrons in the interval $(v, v+dv)$ per c.c.,

$Q_n(v)$=effective cross-section for the excitation of normal atoms to the n-th state and for the collision of v-electron.

If we put, as before,

$$\bar{Q}_n \equiv \frac{\int_{v_n}^{\infty} Q_n(v) v N_e(v) dv}{\int_{v_n}^{\infty} v N_e(v) dv}, \tag{10.3}$$

it becomes

$$\mathfrak{D}_n(T_e) = \bar{Q}_n \cdot \phi_n(T_e), \tag{10.4}$$

with $$\phi_n(T_e) = \int_{v_n}^{\infty} v \cdot \frac{N_e(v)}{N_e} dv.$$

Inserting for $N_e(v)$ the Maxwell expression corresponding to T_e, we have

$$\phi_n(T_e) = 4\left(\frac{k}{2\pi m}\right)^{1/2} T_e^{1/2}\left(1+\frac{\chi_1-\chi_n}{kT_e}\right)e^{-(\chi_1-\chi_n)/kT_e}, \tag{10.5}$$

or, χ's being expressed in e. V.,

$$\phi_n(T_e) = 6.22\times 10^5 T_e^{1/2}\left(1+\frac{11580(\chi_1-\chi_n)}{T_e}\right)e^{-11580(\chi_1-\chi_n)/T_e}. \tag{10.6}$$

§ 11. $Q_n(v)$ increases with v, from zero at the excitation limit v_n.[1] $\bar{Q}_n$ is also a function of T_e; but as in the case of $\bar{Q}$ in the ionization formula, (cf. § 5), we shall approximate it by the following constant values:

n	3	4	5
$\bar{Q}_n$	0.2	0.1	0.06

$\pi a_0^2 = 0.88\times 10^{-16}$ cm^2. being taken as the unit. $\bar{Q}_3$ and $\bar{Q}_4$ have been taken from the data given in the Chap. IV, while $\bar{Q}_5$ has been extrapolated both from those for lower states in our calculations and those for higher velocity impact computed by many authors[2]; yet $\bar{Q}_5$ is fortunately of less importance for the calculation of H_α/H_β.

Both $\mathfrak{C}_n$ and $\mathfrak{D}_n$ have been computed for some values of T_e and are given tabulated as follows:

1. Cf. Chap. IV, Table X.
2. Cf. Bethe, *loc. cit.*

Table II. $\mathfrak{C}({}_nT_e)$ and $\mathfrak{D}_n(T_e)$

n \ T_e	8,000	10,000	12,500	15,000	17,500	20,000	22,500	25,000	30,000
$\mathfrak{C}_n(T_e)\cdot 10^{14}$									
3	5.64	4.80	4.05	3.51	3.09	2.74	2.49	2.28	1.94
4	3.65	3.04	2.52	2.15	1.88	1.66	1.49	1.35	1.13
5	2.52	2.08	1.70	1.43	1.24	1.09	0.97	0.87	0.725
$\mathfrak{D}_n(T_e)\cdot 10^{12}$									
3	0.000	0.015	0.218	1.285	4.64	11.98	24.60	43.3	104.0
4	0.000	0.003	0.059	0.388	1.44	4.03	9.06	16.6	40.7
5	0.000	0.001	0.029	0.196	0.781	2.09	4.68	8.82	22.2

Balmer Decrement

§ 12. The population N_n and the Balmer emission E_n associated with it are connected by

$$E_n = A_{n2} h\nu_{n2} \cdot N_n, \tag{12.1}$$

where A_{n2} represents the probability of spontaneous transition from the n-th to the 2-nd state and ν_{n2} the frequency of the associated emission. The intensity ratio of $H\alpha$ to $H\beta$ is given by

$$\frac{E_3}{E_4} = \frac{A_{32}\nu_{32}}{A_{42}\nu_{42}} \cdot \frac{N_3}{N_4}. \tag{12.2}$$

If we use, as one often does, $H\alpha/H\beta$ instead of E_3/E_4, we have,

$$\frac{H\alpha}{H\beta} = 3.88 \times \frac{N_3}{N_4}. \tag{12.3}$$

Here N's are given by (9.2) in terms of G's, which in turn are given by (10.1). In (10.1), both $\mathfrak{C}$ and $\mathfrak{D}$ are functions of T_e only; however, to construct G by adding them, $\mathfrak{C}$ must be multiplied by the degree of ionization N_e/N_1, so that the Balmer decrement depends, in general, not only on T_e but also on T_*, δ, implicitly through N_e/N_1. In a special case, where either $\mathfrak{C}$ or $\mathfrak{D}$ is negligible, relative values of G's, and consequently of N's, and therefore $H\alpha/H\beta$, are all dependent solely on T_e.

II. Applications to the Model Nebulae

§ 13. In this chapter we will apply the result of our theory to the observed nebulae. For this purpose the objects are in general too remote and faint to enable us to make sufficient observation thereof, and therefore we must satisfy ourselves with some preliminary data.

Observational data on the Balmer decrement have been recently

compiled by Berman[1]. He has classified the observed nebulae in three groups, according to the relative brightness of the principal nebular line, N_2, in comparison with $H\beta$, and shown statistically that the brighter the nebulium emission, the steeper is the decrement and the higher the temperature T_* of the unclear star. The data required for our purpose are reproduced from his work in the first six columns of Table III.[2]

Table III.

Group	N_2	$H\alpha$	$H\beta$	$H\gamma$	T_e	T_*	r in A. U.	δ
I	4.37	3.9	1.00	0.45	1,000	60,000	40,000	4.0×10^{16}
II	2.97	—	1.00	0.48	——	45,000	20,000	$3.0_2 \times 10^{15}$
III	1.81	2.77	1.00	0.50	2,500	30,000	10,000	$1.4_5 \times 10^{14}$

The values of T_* in the table have been determined, referring mainly to Zanstra's observation.[3] The radius of nebulae, r, has been derived from distance estimation by Berman[1], combined with H. D. Curtis' measurement of the apparent diameter[4]; although its values show a considerable dispersion among the individual objects in each group, we have, for definiteness, adopted the figures as in the table. As to the dilution factor δ, assuming with Zanstra[3], $M_* = 0.0^m$, for the absolute bolometric magnitude of the nuclear star, we can determine the radius of the central star r_* by the well-known formula:

$$\log_{10} r_*/r_\odot = 8.5 - 2.\log_{10} T_*,$$

where $r_\odot$ is that of the Sun; thus combined with r above adopted, it determines $\delta = 4r^2/r_*^2$, of which the values are tabulated in the last column.

§ 14. From (12.3), (9.2) and (10.1), by means of Tables I and II, we can now derive the Balmer decrement for each group, taking T_e as a parameter. Results of calculations are summarized in Tables IV and V, and illustrated in Fig. 1.

In Table IV, we have calculated, besides G, the quantity

$$R_n(T_e) \equiv \mathfrak{D}_n(T_e) \Big/ \frac{Ne}{N_1} \mathfrak{C}_n(T_e), \qquad (14.1)$$

which indicates, in a certain sense, the relative importance of collision

1. Berman, *loc. cit.*

2. As to T_e, which has been estimated by Page from the intensity distribution of the continuous Balmer emission, some discussions will be deferred to § 23.

3. Zanstra, *loc. cit.*

4. H. D. Curtis, Publ. Lick Obs. **13** (1918) Part II.

Table IV.

	Te	8,000	10,000	12,500	15,000	17,500	20,000	22,500	25,000
Group I	N_e/N_1	0.63	0.68	0.71	0.77	0.80	0.90	1.09	1.44
	G_3	0.814	0.804	0.775	1.10	2.05	4.68	10.72	24.2
	R_3		0.003	0.08	0.48	1.88	4.8	9.0	13.2
	G_4	0.529	0.506	0.473	0.565	0.846	1.79	4.19	9.61
	R_4		0.001	0.03	0.23	0.96	2.7	5.6	8.6
	G_5	0.360	0.348	0.320	0.360	0.510	0.995	2.25	5.21
	R_5		0.001	0.02	0.18	0.79	2.1	4.4	7.0
Group II	Ne/N_1	1.20	1.31	1.36	1.49	1.80	2.13	2.58	3.96
	G_3	2.96	2.97	2.75	3.48	6.58	13.62	28.8	74.5
	R_3		0.002	0.04	0.25	0.84	2.1	3.8	4.8
	G_4	1.915	1.08	1.71	1.93	3.16	5.80	12.0	31.3
	R_4		0.001	0.02	0.12	0.42	1.14	2.4	3.1
	G_5	1.305	1.28	1.16	1.25	1.93	3.38	6.66	17.5
	R_5			0.01	0.09	0.35	0.9	1.87	2.6
Group III	Ne/N_1	2.14	2.28	2.40	2.54	2.76	3.18	4.18	6.20
	G_3	9.40	8.99	8.40	9.32	13.02	23.7	52.7	128.0
	R_3		0.002	0.02	0.14	0.55	1.37	2.4	3.1
	G_4	6.1	5.69	5.29	5.35	6.55	10.68	23.0	55.6
	R_4		0.001	0.01	0.07	0.28	0.76	1.45	2.0
	G_5	4.16	3.89	3.60	3.49	4.15	6.37	13.14	31.8
	R_5			0.01	0.05	0.23	0.60	1.15	1.63

(G's must be multiplied by 10^{-8} and N_e/N_1 by 10^2.)

Table V. $H\alpha/H\beta$

	Te	8,000	10,000	12,500	15,000	17,500	20,000	22,500	25,000
Group	I	2.91	2.98	3.02	3.42	4.02	4.30	4.21	4.19
	II	2.90	2.96	2.98	3.24	3.74	4.07	4.02	4.00
	III	2.90	2.96	2.965	3.16	3.47	3.77	3.88	3.89

and capture. In Fig. 1, $H\alpha/H\beta$ is represented by thick lines and the ratio R_4 by sharp ones.

The effect of collision is, as is clearly seen from the figure, practically negligible in the region $Te < 12{,}500^\circ$, so that the current (pure capture) theory is applicable; the decrement in this region is so-called "capture-decrement".

Beyond this limit of Te, the collision becomes effective, and $H\alpha/H\beta$ begins to deviate rapidly from the capture-decrement, increasing till it reaches very high value, say ca. 4.3, 4.1 and 3.9 respectively for group

Fig. 1

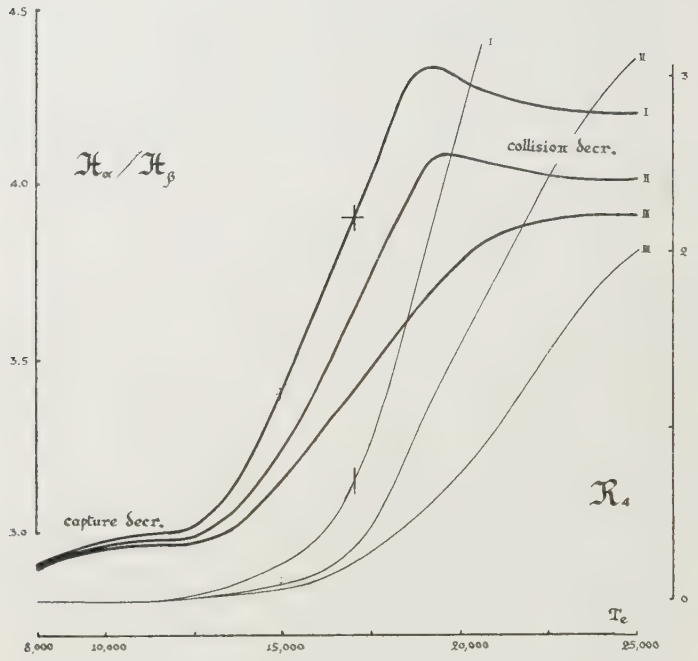

I, II, and III, at about $Te=20{,}000°$. Its highest value may or may not be a maximum, according to the different conditions of the model; but in either case, it approaches asymptotically to a limiting value 3.9 for high temperature over 30,000° (cf. § 15).

In the region $Te=20{,}000°$, the decrement depends chiefly upon the collision; hence we will call it conventionally "collision-decrement" as distinguished from the "capture-decrement".

§ 15. We can determine the electron temperature in nebulae from the observed Balmer decrement. For group I, the observed decrement is steepest, i. e. $Ha/H\beta=3.9$ (cf. Table III). From Table V or Fig. 1, it corresponds $T_e\fallingdotseq 17{,}000°$ and $R_4=0.8$[1].

Such a determination of Te is quite impossible from the pure capture theory; for the decrement in this case is so insensitive to the variation of Te that it is not accountable at all for the observed high decrement of group I (cf. § 1 a). These circumstances may also be understood from the very formula of Cillié[2], which expresses the dependence of

1. Some remarks as to such a high temperature: cf. § 24.
2. Cillié, M. N. **92** (1932) 820, eq. (16).

the capture probability on the velocity of the incoming electron. Parenthetically it may be interesting to refer here to the fact that E. C. G. Stückelberg and P. M. Morse[1], in their probability calculation of slow electrons, have come to the conclusion that relative cross-section of the atom for each state is, in the first approximation, indifferent to the electron velocity.

Now the collision effect not only makes the decrement itself steep but also its dependency on T_e very sensitive, so that the high decrement observed in the nebulae of group I can be accounted for and also the electron temperature thereof can be determined. This comes from the fact that, with increasing quantum number n, the cross-section of the atom decreases more rapidly in the case of collisional excitation than in the case of capture, and moreover this tendency is accelerated by the multiplication of ϕ_n-factor, which is nearly parallel to the number of active electrons.

As for the properties of the "collision-decrement", a clear idea would be obtained if we consider the limiting case where the capture effect is completely excluded. In this case, the decrement has at $T_e \backsim \infty$ a minimum value of 3.9, to which it tends asymptotically, as T_e increases, starting from ∞ at $T_e \backsim 0$. This fact is due to the circumstances, that the diminution of ϕ_n with increasing n is gradually relieved as T_e increases (cf. (10.4)). The curves in Fig. 1 have been obtained by combining both decrements in this case and in the current theory; the relative weights of this combination being the degree of ionization N_e/N_1, on which the behaviour of the curves depends.

Similarly we can treat the groups II and III. In group II, as $H\alpha/H\beta = 3.4$ (Table III), we have $T_e = 16{,}000^\circ$ and $R_4' = 0.2$. The observation for group III fits the capture decrement, so that T_e must be about $12{,}500^\circ$ or less, the collision playing no essential rôle.

§ 16. We have tried in the present chapter, to give the theoretical interpretation of the high decrement observed in groups I and II. Thereby, a method has been found for estimating the electron temperature of the nebula from the observed decrement. But another method of T_e-estimation is suggested from our theory; namely, this can be done by comparing the intensity of any discrete line with that of continuous Balmer emission, as the intensity ratio of these two sorts of emission is intimately connected with R_n (cf. § 22).

1. E. C. G. Stückelberg and P. M. Morse, Phys. Rev. **36** (1930) 16.

Observed value of this ratio is in some nebulae of group I much larger than theoretically predicted by Cillié (cf. § 21); this fact may, however, be reasonably explained, if we reflect upon the circumstances that the collision contributes nothing to the continuous emission, which always remains in a pure capture spectrum (cf. § 1 b).

III. N. G. C. 7662

§ 17. In the preceding chapter we have considered the model nebulae. To be able to apply our theory to the actual nebulae, we must have thorough knowledge on various properties thereof, of which accurate observations are desirable. But only of the bright nebula N. G. C. 7662, have we any considerable amount of data; these have been compiled by T. L. Page[1] and L. Berman[2]. It may be interesting to verify the present theory as applied to this nebula, or to infer some physical conditions in this object from the theory.

The nebula is an object of vis. mag. $8.^m4$, known as "Ring nebula in Andromeda"; its position for 1900 is: $\mathcal{A}R=23^h\ 21.^m1$, $\delta=+41^\circ\ 59'$.

It is a somewhat elongated disc of apparent diameter $14''\times17''$, surrounded by the fragmentally detached faint outer ring of $28''\times32''$. According to Berman (*loc. cit.*) its distance is 1,180 parsecs, so that we get $r=10{,}000$ A. U. for the mean diameter of the inner ring.

The data of spectroscopic observations will be referred to later in due course.

§ 18. The effective temperature T_* of the nucleus star is estimated by various methods; but they are all the same in principle. Among them, the original ones of Zanstra are based on the condition for the continuity of quanta and the equation of energy, viz. the method of hydrogen recombination and that of nebulium excitation. His formulations are as follows[4]:

Method I (hydrogen recombination)

$$\int_{x_1}^{\infty}\frac{x^2}{e^x-1}dx=\sum_{Balmer}\frac{x^3}{e^x-1}A_\nu \tag{18.1}$$

Method II (nebulium excitation)

$$\int_{x_1}^{\infty}\frac{x^3}{e^x-1}dx-x_1\int_{x_1}^{\infty}\frac{x^2}{e^x-1}dx=\sum_{nebulium}\frac{x^4}{e^x-1}A_\nu \tag{18.2}$$

1. Page, *loc. cit.*
2. Berman, *loc. cit.*
3. Curtis, *loc. cit.*
4. Zanstra, *loc. cit.*

$$A_\nu \equiv \frac{L_p}{\nu \dfrac{\partial L_s}{\partial \nu}}, \qquad x \equiv \frac{h\nu}{kT_*},$$

where L_p and L_s are the intensities of the nebular emission and continuous nuclear spectrum. To avoid the intensity L_s, which is very difficult to measure in the technics of observation, R. H. Stoy[1] has proposed another method, combining (18.1) and (18.2):

$$\text{Method III (line ratio)} \quad \frac{\displaystyle\int_{x_1}^{\infty} \frac{x^3}{e^x-1}dx - x_1\int_{x_1}^{\infty}\frac{x^2}{e^x-1}dx}{x'\displaystyle\int_{x_1}^{\infty}\frac{x^2}{e^x-1}dx} = \frac{\displaystyle\sum_{nebulium} L_p}{\displaystyle\sum_{Balmer} L_p\left(\frac{\nu'}{\nu_p}\right)}, \qquad (18.3)$$

where ν' denotes a certain frequency suitably chosen, say, that of H_β, and x' corresponds to ν'.

Page has applied these formulae to his observations[2]; the results are inserted in the second column of Table VI.

Table VI. Nuclear Temperature of N. G. C. 7662.

Method	Direct (Page)	Corrected for collision
I. Hydrogen recombination	73,000°	70,000°
II. Nebulium excitation	67,000	85,000
III. Line ratio	32,000	75,000

§ 19. As is seen from the table, the value derived by the third method seems to be too small compared with the other two, even if the difficulty of the observational technic is taken into account. This discrepancy seems to be removable by introducing a correction for collisional effect.

i) Each term under $\sum$ in (18.1) represents the number of Balmer quanta. This, however, should not be equated to the number of quanta in the ultraviolet region, if the collision effect is not negligible, viz. we have not to take L_p itself, but the very fraction of it, which corresponds to the contribution from capture[3]. For our nebula, it amounts ca. 1/3, because this contribution appears about half that of collision, as is easily inferred from the observation of E_n/Ba_c (cf. § 22). Usually, the continuous Balmer emission is neglected in the summation of quanta. But

1. R. H. Stoy, M. N. **93** (1933) 588.

2. Page, *loc. cit.*

3. When the collisional ionization is effective, this fraction must further be reduced to that part of capture which balances with the photoelectric ionization. But it is not the case in our nebula.

this is not the case in the present consideration ; in fact, it is as large as about 1/2 of the whole discrete Balmer quanta due to capture (cf. C_{nl} in Table X), and consequently the right hand side of (18.1) must be multiplied by $\frac{1}{3}\times 2$. Thus Page's result is reduced to about 70,000°.

ii) As for the second method, each term on the left hand side of (18.2) represents the energy liberated by the spontaneous transition succeeding to the collisional excitation. Thus in our case, where the hydrogen emission does not consist purely of capture spectrum, the summation must be extended to those parts of Balmer and Lyman emission which come from the collisional excitation[1]. To see the order of magnitude of this excitation, we take the contribution from the Balmer emission as $5\times\frac{2}{3}\fallingdotseq 3$, normalizing the intensity of its whole energy to 5 ; that of Lyman α as 30, taking as ten times that of Balmer[2], and the total nebulium emission as 30, twice that of N_1+N_2 (cf. Table III). We should then adopt for the total sum of the nebulium emission $33+30$ instead of 30 ; that is, the second side of the equation (18.2) must be doubled. Consequently, Page's result must be raised to about 85,000°. A discrepancy of 20% may not be so grave, if we remark that T_* is very sensitive for its high value to the variation of A_ν.

iii) The value obtained by the third method has been corrected in the same way, multiplying the numerator by $\frac{1}{3}\times 2$ and the denominator by 2 in the right side of (18.3). The corrected value, 75,000°, seems to lessen the discrepancy.

§ 20. Now we tentatively employ 70,000° for T_*, according to the

Table VII. Theoretical Balmer Decrement for N. G. C. 7662.

T_e	15,000	17,500	20,000	22.500	25.000	30,000
N_e/N_1 $\times 10^{-2}$	3.9	3.78	4.00	4.42	5.12	7.52
$H\alpha/H\beta$	3.12	3.36	3.68	3.85	3.95	4.04
R_3	0.09	0.40	1.09	2.24	3.71	7.11
R_4	0.05	0.20	0.605	1.31	2.40	4.79
R_5	0.04	0.17	0.48	1.09	1.98	4.07

1. This means that the dissipation of the kinetic energy of the electron is caused by the inelastic collision not only with nebulium elements but also with hydrogen atom. (also cf. foot-note 3 of the preceding page.)

2. Contributions from higher series are all neglected, owing to the smallness of their energy.

discussion in the preceding paragraph. Then, we obtain as the dilution factor $\frac{I}{\delta} = 2.25 \times 10^{-16}$, assuming $M_* = 0.^m0$ as before (cf. § 13).

Then, we are able to calculate the Balmer decrement from (12.3), (9.2), and (10.1), taking T_e as a parameter. The results are given in Table VII and illustrated in Fig. 2.

Fig. 2. N. G. C. 7662

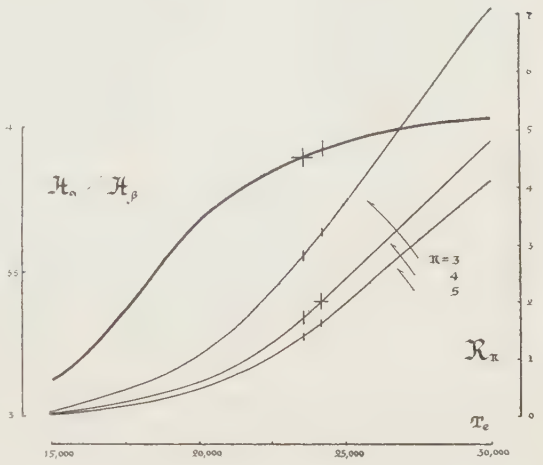

§ 21. The electron temperature T_e can be determined either from the observed Balmer decrement or from the intensity ratio of the discrete to the continuous Balmer emission. The observed data are as in Table VIII.

Table VIII. Observed Balmer Decrement of N. G. C. 7662.

	Balmer decrement	$\log_{10} E_n/Ba_e$						
		Observational (Page)		Theoretical (Cillié)				
		W 4.9″	E 4.9″	1,000°	5,000°	10,000°	20,000°	50,000°
N_2	3.66							
$H\alpha$	(3.91)	— —	——	——	3.38	3.60	3.77	3.98
$H\beta$	1.0	4.02	3.76	2.40	2.95	3.14	3.31	3.50
$H\gamma$	0.45	3.67	3.41	2.13	2.65	2.84	3.00	3.14
$H\delta$	0.23	3.38	3.12	1.92	2.42	2.60	2.74	2.91

In the table, the values of Balmer decrement are those of Berman[1], which have been corrected by him for space reddening. $H\alpha$ is absent, but if we judge from the intensities of $H\gamma$ and $H\delta$, it seems to bear the character of collisional decrement. Thus we will assume for it the mean value of the first group (cf. Table I).

Table VIII also contains the intensity ratio of the discrete Balmer E_n to the continuous emission Ba_e per unit frequency at the series limit.

1. Berman, *loc. cit.*

Here the observed values are not the original ones of Page[1], who observed the continuous emission at 4.9″ West and East of the nucleus, but those obtained after correcting for space reddening, according to the Berman's formula.

Theoretical ratio is due to Cillié[2], who derived it as follows :—The energy emitted per sec. per c.c. in a frequency range $(\nu, \nu+d\nu)$ beyond the series limit is given by

$$N_e^2 \frac{2^6\pi^5}{(6\pi)^{3/2}} \cdot \frac{\varepsilon^{10}}{m^2c^3h^2} \left(\frac{m}{kT_e}\right)^{3/2} e^{(\chi_2-h\nu)/kT_e} d\nu.$$

At the head of the series limit, it becomes per unit wave number

$$Ba_e = [\overline{23}\cdot 902] N_e^2 / T_e^{3/2}.$$

Combining it with (12.1), he found

$$\frac{E_n}{Ba_e} = [22\cdot 098] \frac{N_n}{N_e^2} A_{n2} h\nu_{n2} T_e^{3/2}. \qquad (21.1)$$

§ 22. In the case of pure capture spectrum, N_n/N_e^2 is uniquely determined by (9.2) and (10.1) as a function of T_e. For our nebula, the collision, as will be found later, does not yet affect the degree of ionization, so that the denominator remains the same as Cillié's value for it. Therefore only N_n increases with T_e. But the observed ratio is about 3 times that given by (21.1) for $T_e = 20{,}000°$; and thus it is suggested N_n must be raised by the same factor. Hence we may conclude that the collisional excitation surpasses about twice that of capture[3]; thus we may roughly take for $n=4$, $R_4=2$, which corresponds to $T_e = 24{,}500°$ and $H\alpha/H\beta = 3.93$. On the contrary, if we start from the decrement, its value 3.9 gives $T_e = 23{,}500°$ and $R_4 = 1.7$. The accordance of the above results may be permitted as satisfactory, if we reflect upon the approximate nature of our method and various difficulties on the observational side.

§ 23. The intensity distribution of the continuous Balmer emission led Page to a conclusion of much lower temperature (1,200°–4,000° for the present nebula) than ours; it moreover suggests a non-Maxwellian distribution of the electron velocities in the nebula (cf. § 1 c and d). As an approach to the explanation of this anomaly, it is suggested that slow electrons created by the inelastic collision are captured[4], before they are adjusted to the thermal velocity, disturbing the Maxwellian distri-

1. Page, *loc. cit.*
2. Cillié, *loc. cit.*
3. In fact, G_n is the main term for N_n (cf. (9.2)).
4. The capture probability is inversely proportional to the kinetic energy of the colliding electron.

bution. They may be effective in the direct vicinity of the series limit and be able to change the slope of the continuous emission[1]; though they can, by no means, affect the whole amount of capture. In other words, it may happen in the nebula that the velocity distribution *effective for capture* is non-Maxwellian.

§ 24. *Metastability of 2S state.* In the preceding paragraphs, we have been concerned only with the principal quantum number n, neglecting all the finer structure of hydrogen atom. Especially, we have pretended ignorance on the metastability of $2S$ state, which may have caused an accumulation of atoms in this level and may therefore have violated our starting assumption of the transparency of the nebula to the subordinate lines[2].

In N. G. C. 7662, for example, there are 500×6 electrons per c.c. (cf. Table VIII), but among them only 1% have energy enough to excite the atom to $2S$ state: thus there are 30 active electrons and 6 normal atoms per c.c. If we assume 2×10^8 cm. sec.$^{-1}$ as the mean electron velocity and $\pi a_0^2 \fallingdotseq 10^{-16}$ cm^2, as the effective cross-section (cf. Table X), we get for the frequency of such excitations, $30\times2\times10^8\times10^{-16}=6\times10^{-7}$ sec.$^{-1}$ On the other hand, the spontaneous transition occurs once every several months[3] or with the frequency of the order 10^{-7} sec., a figure which is rather smaller than the former. Thus if we put aside for a moment the removal of atoms from $2S$ state by quantum absorption, it may be concluded that the population N_{2S} is mainly adjusted by balancing the excitation $1S\rightarrow2S$ against the de-excitation $2S\rightarrow1S$ through the collisional processes; that is N_{2S} obeys Boltzmann's law:

$$\frac{N_{2S}}{N_{1S}}=e^{-h(\chi_1-\chi_2)/kT_e},$$

the values of which are given in the second row of the following table.

T_e	10,000	15,000	20,000	25,000	30,000
N_{2S}/N_{1S}	7.8×10^{-6}	3.9×10^{-4}	2.8×10^{-3}	0.91×10^{-2}	2.0×10^{-2}
$\omega_{2S,3P}\cdot N_{2S}/N_{1S}$	1.6	7.9×10	5.6×10^2	1.8×10^3	4.0×10^3

According to the usual notation, let $\omega_{2S,3P}$ be the ratio of the absorption coefficient for $2S$–$3P$ of H_α to that of ultraviolet radiation

1. If so, in the comparison of the discrete to the continuous emission (§ 21), it would not be preferable to make use of the intensity of continuous emission at the series limit. It is best to use the integrated emission beyond the series limit, but may be difficult observationally as an actual problem.

2. As for the self-reversal, M. Kurihara has exhaustively discussed the nature of this effect in the case of B_e stars; (these Memoirs **21** (1938) 89.)

3. Bethe, *loc. cit.* § 43.

beyond the Lyman limit. As it depends slightly on T_e and T_*, we will put $\omega_{2S,3P}=2\times 10^5$, with M. Kurihara[1]. In our investigation we have assumed that the optical depth is unity for the ultraviolet radiation, so that $\omega_{2S,3P}\frac{N_{2S}}{N_{1S}}$ represents directly the optical depth for $2S$–$3P$ of $H\alpha$. For $T_e<10{,}000^\circ$, $\omega_{2S,3P}\frac{N_{2S}}{N_{1S}}<1$ as shown in the above table. Therefore the nebula may be considered as transparent to $H\alpha$ in this case. Thus so far as the nebulae of group III are concerned, our assumption of transparency is justified. But this is not the case for the other groups; there it seems, indeed, that the absorptions take place from the $2S$ state.

§ 25. So far we have treated the atom as an isolated existence. But at the same time we have to take account of the influences of the environment; its disturbances cause, more or less, the mutual coherences of pure states, and thus the metastable state has a tendency to lose its proper character. As for such external influences, there are in our case powerful mechanisms, which remove the atom from $2S$ state.

i) The transition $2^2S_{1/2}\rightarrow 2^2P_{1/2}$ is induced by the electron impact. The effective area for the mechanism can be estimated in the same way as in Chap. IV; a rough calculation shows that it amounts to at least 100, perhaps 10^4 times that of de-excitation (of the order πa_0^2). Thus the values of N_{2S}/N_{1S} given above may be reduced by the same ratio.

ii) There is a sort of Stark effect caused by the electric field due to the surrounding free electrons and protons. There the disturbed wave functions are given by the linear combinations of $2^2S_{1/2}$- and $2^2P_{1/2}$-state. Thus $2^2S_{1/2}$-state loses its metastability[3]; the transition probability to $1^2S_{1/2}$-state becomes in our case of the order 1 sec.$^{-1}$ Therefore, if only this effect is considered, the population N_{2S} is given roughly by

$$\frac{N_{2S}}{N_{1S}}\fallingdotseq\frac{6\times 10^{-7}}{1}\fallingdotseq 10^{-6}.$$

Therefore

$$\omega_{2S,3P}\frac{N_{2S}}{N_{1S}}<1.$$

These circumstances would prevent the accumulation of atoms in that very state.

§ 26. Some authors[4] have suggested that considerable amount of atoms may be accumulated to $2P$ state, owing to the large density of

1. M. Kurihara, *loc. cit.*
2. Bethe, *loc. cit.* § 43.
3. Cf. Bethe, *loc. cit.* especially § 43.
4. Ambarzumian, Cillié, Page, Berman, *loc. cit.*

L_α-radiation. But simple estimation shows that this radiation is not so dense as to cause the self-reversal of Balmer lines. Indeed, Ambarzumian[1], in his order-estimation of this effect, has employed as the dilution factor $\delta = 10^{13}$ for $T_* = 40{,}000^\circ - 50{,}000^\circ$, which seems, however, to be too small (cf. Table III). If we adopt our correct value $\delta = 10^{15}$, the population of atoms in $2P$ state is reduced to 1/100 of his value. Thus it becomes $N_{2P}/N_{1S} \fallingdotseq 5 \times 10^{-7}$, which makes the optical depth $\omega_{2P,3D}\frac{N_{2P}}{N_{1S}}$ smaller than unity.

IV. Excitation of Hydrogen Atom by Slow Electron Impact

The collisional excitation of hydrogen atom immediately interesting to the nebular condition is the case of slow electron impact; indeed, electrons have in the nebula very slow thermal velocity, so that few of them exceed the limit of Lyman series, 13.53 e. V. The effective cross-section for excitation can be easily estimated, if the electron velocity corresponds to 100 e. V. or more. For slow collision, however, we must treat very complicated expressions, since both the distortion of electron wave and the exchange effect between colliding and atomic electrons become large.

In this chapter we will try to make an order-estimation in such a case, neglecting all but the effect of exchange; the method is in principle the same as that of Massey and Mohr.[2]

§ 27. *Effective cross-section.* We treat the problem statically and start with Schrödinger's equation for the system of two electrons:

$$(\Gamma_1^2 + \Gamma_2^2)\Psi(\boldsymbol{r}_1, \boldsymbol{r}_2) + \frac{8\pi^2 m}{h^2}\left(E_1 + E_2 - \varepsilon^2\left[\left(\frac{1}{r_{12}} - \frac{1}{r_1}\right) - \frac{1}{r_2}\right]\right)\Psi(\boldsymbol{r}_1, \boldsymbol{r}_2) = 0, \tag{27.1}$$

where suffixes 1 and 2 are referred to the colliding and atomic electrons respectively, and ε means the elementary charge, and r_{12}, the distance between two electrons.

As a first approximation, the atomic electron must satisfy the wave equation of hydrogen:

$$\Gamma_2^2\psi(\boldsymbol{r}_2) + \frac{8\pi^2 m}{h^2}\left(E_2 + \frac{\varepsilon^2}{r_2}\right)\psi(\boldsymbol{r}_2) = 0. \tag{27.2}$$

---

1. Ambarzumian, *loc. cit.*
2. Mott, Proc. Roy. Soc. **125** (1929) 222.
   Massey and Mohr, ibid. **132** (1931) 605, **136** (1932) 289, **139** (1933) 187, **140** (1933) 613, **146** (1934) 880.

Let $\psi_N(\boldsymbol{r}_2)$ be a solution of this equation, viz. an eigen-function corresponding to the energy level χ_N, each quantum state (n, l, m) being represented by a single letter N.

Suppose now for a moment, two electrons are distinguishable and seek solution of such a form as

$$\Psi(\boldsymbol{r}_1, \boldsymbol{r}_2)=(\sum+\int)_N\psi_N(\boldsymbol{r}_2)F_N(\boldsymbol{r}_1), \tag{27.3}$$

in which for large r holds

$$F_N(\boldsymbol{r})\sim e^{ik_1z}+\frac{e^{ik_1r}}{r}f_I(\theta) \quad \text{for normal state, } N=I,$$

$$\sim \frac{e^{ik_Nr}}{r}f_N(\theta) \quad \text{otherwise.} \tag{27.4}$$

By summation and integration in (27.3) are included both all the discrete and the continuous state N; and

$$k_1=\frac{2\pi mv_1}{h}, \qquad k_N^2=\frac{8\pi^2m}{h^2}[E_1-(\chi_N-\chi_I)]=\left(\frac{2\pi mv_N}{h}\right)^2; \tag{27.5}$$

thus e^{ik_1z} means the incident electron wave of velocity v_1 along z-axis and of unit density per c.c. and the scattered electron after the excitation of the atom in its N-th state is represented by the spherical wave $r^{-1}e^{ik_Nr}f_N(\theta)$, where θ is the angle of scattering (Fig. 3).

Fig. 3 Direct Excitation

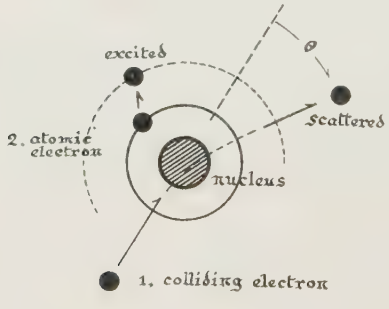

Fig. 4 Exchange Effect

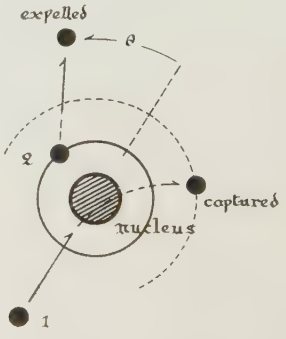

Then, if the incident beam is such that one electron falls on cm^2, per sec., the number of electrons $I_N(\theta)d\omega$, which are scattered with velocity v_N into an angle element $d\omega$ per sec. is given by

$$I_N(\theta)d\omega=\frac{v_N}{v_1}|f_N(\theta)|^2=\frac{k_N}{k_1}|f_N(\theta)|^2. \tag{27.6}$$

Now, we define the total cross-section as

$$Q_N\equiv\int I_N(\theta)d\omega=2\pi\int_0^\pi I_N(\theta)\sin\theta d\theta. \tag{27.7}$$

Now, it follows from (27.1) and (27.3), taking account of (27.2),

$$(\sum+\int)_N\psi_N(\boldsymbol{r}_2)\left[\nabla_1^2+\frac{8\pi^2m}{h^2}(E_1+E_2-(\chi_N-\chi_I))\right]F_N(\boldsymbol{r}_1)$$
$$=\frac{8\pi^2m}{h^2}\left[\varepsilon^2\left(\frac{1}{r_{12}}-\frac{1}{r_1}\right)\right]\Psi(\boldsymbol{r}_1,\boldsymbol{r}_2);$$

multiplying it by $\psi_N^*(\boldsymbol{r}_2)$ and integrating over the whole $\boldsymbol{r}_2$ space,

$$(\nabla_1^2+k_N^2)F_N(\boldsymbol{r}_1)=\frac{8\pi^2m}{h^2}\int\varepsilon^2\left(\frac{1}{r_{12}}-\frac{1}{r_1}\right)\Psi(\boldsymbol{r}_1,\boldsymbol{r}_2)\psi_N^*(\boldsymbol{r}_2)d\tau_2. \qquad (27.8)$$

§28. *Exchange effect.* When the eigen-function corresponds to the continuous state, it also gives some information about the probability that the incident electron is captured and the atomic electron ejected (Fig. 4). But in order to see it more clearly, we expand (27.3) in the alternative form:

$$\Psi(\boldsymbol{r}_1,\boldsymbol{r}_2)=(\sum+\int)_N\psi_N(\boldsymbol{r}_1)G_N(\boldsymbol{r}_2), \qquad (28.1)$$

assuming that G_N has the asymptotic form:

$$G_N\sim\frac{e^{ik_Nr}}{r}g_N(\theta) \qquad \text{for large } r. \qquad (28.2)$$

Then, in the same way as before, we obtain the equation for G_N:

$$(\nabla_2^2+k_N^2)G_N(\boldsymbol{r}_2)=\frac{8\pi^2m}{h^2}\int\varepsilon^2\left(\frac{1}{r_{12}}-\frac{1}{r_2}\right)\Psi(\boldsymbol{r}_1,\boldsymbol{r}_2)\psi_N^*(\boldsymbol{r}_1)d\tau_1. \qquad (28.3)$$

Equations (27.8) and (28.3) determine the function F_N and G_N.

§29. As $\Psi(\boldsymbol{r}_1,\boldsymbol{r}_2)$ contains F_N and G_N, the equations (27.8) and (28.3) are of integro-differential type. They are easily reduced to the integral equation. But it is still difficult to obtain their strict solutions; hence some adequate approximation to $\Psi(\boldsymbol{r}_1,\boldsymbol{r}_2)$ is required.

The following calculations are based on the *Born's approximation*; that is, neglecting all the disturbances of electron waves and of the atomic field, we take for $\Psi(\boldsymbol{r}_1,\boldsymbol{r}_2)$ the following form:

$$\Psi(\boldsymbol{r}_1,\boldsymbol{r}_2)=e^{ik_1\boldsymbol{n}_0\boldsymbol{r}_1}\psi_I(\boldsymbol{r}_2), \qquad (29.1)$$

where $\boldsymbol{n}_0$ is the unit vector in the direction of positive z-axis. Then (27.8) and (28.3) become

$$(\nabla_1^2+k_N^2)F_N(\boldsymbol{r}_1)=\frac{8\pi^2m\varepsilon^2}{h^2}\int\left(\frac{1}{r_{12}}-\frac{1}{r_1}\right)e^{ik_1\boldsymbol{n}_0\boldsymbol{r}_1}\psi_I(\boldsymbol{r}_2)\psi_N^*(\boldsymbol{r}_2)d\tau_2. \qquad (29.2)$$

$$(\nabla_2^2+k_N^2)G_N(\boldsymbol{r}_2)=\frac{8\pi^2m\varepsilon^2}{h^2}\int\left(\frac{1}{r_{12}}-\frac{1}{r_2}\right)e^{ik_1\boldsymbol{n}_0\boldsymbol{r}_1}\psi_I(\boldsymbol{r}_2)\psi_N^*(\boldsymbol{r}_1)d\tau_1. \qquad (29.3)$$

In the integration of (29.2), the term coming from $1/r_1$ vanishes owing to the orthogonality of the wave functions.

The solutions for F_N and G_N are obtained by applying Green's theorem, viz. we get, for large r,

$$F_N(\boldsymbol{r}) \sim \frac{e^{ik_N r}}{r} f_N(\theta),$$

$$G_N(\boldsymbol{r}) \sim \frac{e^{ik_N r}}{r} g_N(\theta),$$

with

$$f_N(\theta) = \frac{2\pi m\varepsilon^2}{h^2} \iint e^{i(k_1 \boldsymbol{n}_0 - k_N \boldsymbol{n})\boldsymbol{r}_1} \left(\frac{-1}{r_{12}}\right) \psi_I(\boldsymbol{r}_2) \psi_N^*(\boldsymbol{r}_2) d\tau_1 d\tau_2, \tag{29.4}$$

$$g_N(\theta) = \frac{2\pi m\varepsilon^2}{h^2} \iint e^{i(k_1 \boldsymbol{n}_0 \boldsymbol{r}_1 - k_N \boldsymbol{n} \boldsymbol{r}_2)} \left(\frac{1}{r_2} - \frac{1}{r_{12}}\right) \psi_I(\boldsymbol{r}_2) \psi_N^*(\boldsymbol{r}_1) d\tau_1 d\tau_2, \tag{29.5}$$

where $\boldsymbol{n}$ is the unit vector in the direction of $\boldsymbol{r}$.

§ 30. So far, we have assumed that the two electrons are distinguishable. Now we introduce the condition that they are indistinguishable and obey Fermi-Dirac's statistics; then, for the unpolarized beam of the impinging electrons, both the functions f_N and g_N are combined to give the scattering intensity as

$$I_N(\theta) d\omega = \frac{k_N}{k_1} \left[\frac{3}{4} |f_N(\theta) - g_N(\theta)|^2 + \frac{1}{4} |f_N(\theta) + g_N(\theta)|^2 \right] d\omega, \tag{30.1}$$

and Q_N is given by (27.7).

Final formulae and Numerical results

§ 31. If the reduction of our formulae is treated in detail, it will be easily seen that the states with negative magnetic quantum number ($m < 0$) have the same excitation probabilities as the positive ones. Consequently we restrict ourselves to the case $m \geqslant 0$.

The normalized wave function for hydrogen is[1]

$$\psi_N = \psi_{nlm} = N_{nlm} \left(\frac{2r}{na_0}\right)^l e^{-r/na_0} L_{n+l}^{2l+1}\left(\frac{2r}{na_0}\right) \bar{P}_l^m(\cos\theta)\ e^{im\phi}$$

$$N_{nlm} = \frac{1}{\sqrt{4\pi}} \frac{\left(\frac{2}{na_0}\right)^{3/2}}{(n+l)!} \sqrt{\frac{(n-l-1)!}{(n+l)!\, n}}, \tag{31.1}$$

where L's are Laguerr polynomials and $\bar{P}$'s normalized spherical harmonics.

Now, we have to insert these expressions in (29.4) and (29.5).

§ 32. For $f_N(\theta)$, after some complicated mathematical reductions we obtain finally

$$f_N(\theta) = \sqrt{\pi}\, a_0 \cdot \Theta_n(\theta) \Omega_{nlm} \bar{P}_l^m(\cos\psi) I_{nl}(\zeta), \tag{32.1}$$

1. Cf. Condon and Shortley, The Theory of Atomic Spectra. (1935) Chap. V.

with

$$\cos\psi=(k_1-k_n\cos\theta)/K$$
$$K^2=k_1^2+k_n^2-2k_1k_n\cos\theta$$
$$\Theta_{lm}(\theta)=(a_0K)^{-5/2}$$
$$\Omega_{nlm}=i^{l+m+2}\frac{1}{(n+l)!}\sqrt{2n\frac{(n-l-1)!}{(n+l)!}}$$
$$\zeta=\frac{na_0}{2}K \qquad (32.2)$$
$$I_{nl}(\zeta)=\int_0^\infty e^{-\xi(1+n)/2}\xi^{l+3/2}L_{n+l}^{2l+1}(\xi)J_{l+1/2}(\zeta\xi)d\xi \qquad (32.3)$$

where J's are Bessel functions. Integrals (32.3) can be evaluated elementarily and their values are given in Table IX.

Table IX.

(n,l)	$-\sqrt{\frac{\pi}{2}}\cdot I_{nl}(\zeta)$	$-\sqrt{\frac{\pi}{2}}\cdot I_{nl}^{\circ}(\zeta)$
(2,0)	$16\zeta^{5/2}\left(\frac{9}{4}+\zeta^2\right)^{-3}$	$2\zeta^{1/2}(4\zeta^2-1)\left(\frac{1}{4}+\zeta^2\right)^{-3}$
(2,1)	$72\zeta^{5/2}\left(\frac{9}{4}+\zeta^2\right)^{-3}$	$24\zeta^{3/2}\left(\frac{1}{4}+\zeta^2\right)^{-3}$
(3,0)	$36\zeta^{5/2}(3\zeta^2+4)(4+\zeta^2)^{-4}$	$9\zeta^{1/2}\left(6\zeta^4-4\zeta^2+\frac{3}{8}\right)\left(\frac{1}{4}+\zeta^2\right)^{-4}$
(3,1)	$576\zeta^{3/2}(3\zeta^2+4)(4+\zeta^2)^{-4}$	$144\zeta^{3/2}(4\zeta^2-1)\left(\frac{1}{4}+\zeta^2\right)^{-4}$
(3,2)	$11520\zeta^{5/2}(4+\zeta^2)^{-4}$	$2880\zeta^{5/2}\left(\frac{1}{4}+\zeta^2\right)^{-4}$
(4,0)	$48\zeta^{5/2}(16\zeta^4+13\zeta^2+575)\left(\frac{25}{4}+\zeta^2\right)^{-5}$	$\zeta^{1/2}(384\zeta^6-672\zeta^4+168\zeta^2+21)\left(\frac{1}{4}+\zeta^2\right)^{-5}$
(4,1)	$1800\zeta^{3/2}(16\zeta^4+88\zeta^2+125)\left(\frac{25}{4}+\zeta^2\right)^{-5}$	$120\zeta^{3/2}(80\zeta^4-56\zeta^2+5)\left(\frac{1}{4}+\zeta^2\right)^{-5}$
(4,2)	$69120\zeta^{5/2}(8\zeta^2+25)\left(\frac{25}{4}+\zeta^2\right)^{-5}$	$34560\zeta^{5/2}(4\zeta^2-1)\left(\frac{1}{4}+\zeta^2\right)^{-5}$
(4,3)	$4838400\zeta^{7/2}\left(\frac{25}{4}+\zeta^2\right)^{-5}$	$967680\zeta^{7/2}\left(\frac{1}{4}+\zeta^2\right)^{-5}$

§ 33. Reduction of $g_N(\theta)$ is much more complicated. To avoid laborious calculations, we introduce the following approximations:

i) *Slow collision*: Close above the excitation potential, k_N is small compared with k_1, namely, the colliding electron dissipates most of its kinetic energy in exciting the atom. We may, therefore, neglect k_N in the exponential factor of (29.5), thus the g_N-terms become independent of the scattering angle θ and the excitation probability vanishes owing to the factor $e^{-im\phi}$, except $m=0$.

$$g_N(\theta)=\sqrt{\pi}\,a_0\cdot\eta^{-1/2}\Xi_{nl}I_{nl}(\eta),\qquad m=0 \tag{33.1}$$

$$\eta=\frac{na_0}{2}k_1$$

$$\Xi_{nl}=i^{l+2}\frac{n}{(n+l)!}\sqrt{\frac{2l+1}{2}\cdot\frac{(n-l-1)!}{(n+l)!}}. \tag{33.2}$$

Here, the extra term coming from $1/r_2$ in the brackets of (29.5) has been omitted, though it surpasses the retained term (33.1) in the present case. It is, indeed, as in the case of $f_N(\theta)$, a term, which ought to vanish if the exact expression was employed for the wave function of incoming electron instead of plane wave approximation. The discrepancy may originate from the circumstances that the neglection of k_N means, in fact, for this term, complete omission of the phase factor for the second electron.

ii) *Moderate velocity collision*: Though of no direct use, we will here deal with this case for the sake of completeness. Now, the integral value of (29.5) comes mainly from the domain where r_1 and r_2 are small, so that we may put $e^{-r_2/a_0}=1$ in $\psi_I(\boldsymbol{r}_2)$. Then we get

$$g_N(\theta)=\sqrt{\pi}\,a_0\cdot\Theta_n^0(\theta)\Omega_{nlm}\bar{P}_l^m(\cos\psi)I_{nl}^0(\zeta), \tag{33.3}$$

$$\Theta_n^0=(a_0K)^{-1/2}(a_0k_n)^{-2}, \tag{33.4}$$

Table X. $Q_{nl}(v)$ and C_{nl}

(n,l) v	$Q_{nl}(v)$							C_{nl}
	1.95	2.0	2.1	2.2	2.3	2.4	2.5	
$1S$								0.227
1								0.227
$2S$	0.14	0.18	0.23	0.26	0.29	0.31	0.32	0.0335
$2P$	0.46	0.63	0.88	1.07	1.26	1.30	1.38	0.109
2	0.60	0.81	1.11	1.33	1.55	1.61	1.70	0.143
$3S$			0.024	0.041	0.051	0.058	0.064	0.0114
$3P$			0.077	0.13	0.19	0.22	0.26	0.0403
$3D$			0.0084	0.016	0.021	0.024	0.026	0.0520
3			0.109	0.187	0.261	0.302	0.350	0.104
$4S$				0.022	0.032	0.039	0.046	0.0053
$4P$				0.042	0.061	0.072	0.084	0.0190
$4D$				0.0072	0.0089	0.011	0.012	0.0318
$4F$				—	—	—	—	0.0254
4				0.071	0.102	0.122	0.142	0.0814

$$I_{nl}^{0}(\zeta)=\int_{0}^{\infty} e^{-\frac{1}{2}(\xi+\zeta)}\xi^{l+\frac{1}{2}}L_{n+l}^{2l+1}(\xi)J_{l+1/2}(\zeta\xi)d\xi. \qquad (33.5)$$

Thus elementary integration is also possible as in (32.3). Final expressions are shown in Table IX.

§ 34. *Numerical results.* We can now calculate the cross-section Q_N, integrating $I_N(\theta)$ over all directions, which, in turn, is given by f_N and g_N in (29.4) and (29.5), and by k_N in (27.5).

Rough calculations were performed and reproduced in Table X. As for the absolute values, only their orders must be consulted, but their relative values for different states N may be rather accurate.

In the table, cross-section $Q_{nl}(v)$ is given in units of πa_0^2, and v in 1000 km. per sec. We have also inserted recombination probabilities, which have been taken from Stückelberg and Morse's paper[1]. There, a quantity C_{nl} is defined by the formula of cross-section : $q_{nl}=C_{nl}\cdot 10^{-20}/V$, V being the electron velocity in volts.

Summary

It has been pointed out that the effect of collisional excitation of normal hydrogen atoms cannot be disregarded in the emission mechanism of the Balmer lines in the planetary nebulae ; that it accounts for the high decrement of Balmer emission and that it gives at the same time, a definite idea of the electron temperature.

(I) 1) In §§ 3–5, the current formula of ionization is modified in order to include the collision effect ; the modified formula changes slightly the degree of ionization in the nebular conditions (§ 6).

2) In connection with this, we have discussed the velocity distribution of the electrons in details, and concluded that it must obey the Maxwellian law, at least in close approximation (§ 7).

3) Cillié's equation has been modified to include the effect of collisional excitation in §§ 8–11.

(II) 4) Using the formulae above obtained, Balmer decrements have been derived for model planetary nebulae, which are chosen so as to correspond to Berman's classification. Theoretical decrement changes from 2.9 to 4.3 with electron temperature in agreement with observations (§§ 13 & 14).

5) Balmer decrement is sensitively connected with the electron temperature, so that the observed decrement fixes the latter. It falls between 10,000°–25,000° for most nebulae (§ 14).

1. Stückelberg and Morse, *loc. cit.*

(III) In connection with Page's observations of the continuous Balmer emission, detailed discussions have been made about N. G. C. 7662, especially about various questions which arose about it.

6) Discrete Balmer emission is a mixture of capture and collision spectra, while the continuous Balmer emission always remains in a pure capture spectrum. From this point of view, a correction has been made of the Zanstra and Stoy methods of determination of nuclear temperature, and applied to the same nebula N. G. C. 7662 (§§ 18 & 19). Thus it seems that the systematic discrepancy between Zanstra's estimate and Stoy's is improved.

7) That the Balmer continuous emission appears fainter than has been expected from the recombination theory has been also explained from the same point of view (§§ 16, 21 & 22).

8) Finally our starting assumption that the nebula is transparent to the subordinate lines has been criticized: (i) the metastability of $2S$ state loses its proper character, owing to the disturbances from the outer fields (§§ 24 & 25); (ii) the accumulation of atoms in $2P$ state due to the denseness of Lyman α radiation, seems not to be so large as to cause the self-reversal.

(IV) In Chap. IV, the excitation of the normal hydrogen atom by slow electron impact has been treated wave-mechanically; the method of approximation has been explained and the final formulae with their numerical results have been given.

I take pleasure in expressing my hearty thanks to Prof. Dr. Toschima Araki for his active guidance and constant encouragement, to Dr. Michinori Kurihara for his many valuable criticisms of the present work, and to Surgeon-Captain M. Nobé and Surgeon-Lieutenant Y. Uématu, who took special care of my health and gave permission to undertake this work during my military service in the summer of 1937. Finally I must acknowledge my deep indebtness for the fund from *Hattori Hôkôkwaï*.

Institute for Astrophysics,
Kyoto Imperial University,
March 1938.

An Investigation of Earth Currents on the Volcano Aso

Part I. The Potential Difference of the Upward Earth-current flowing toward the top of a Volcano

By **Munetosi Namba**

(Received Sept. 13, 1938)

Abstract

It is a well known fact that there is always a certain definite ascending current along an inclined earth surface. The writer has measured the distributions of the potential gradient of the earth current near the mountain tops of several volcanic cones, and arrived at the conclusion that the ascending current of a cinder cone is mainly due to the streaming potential caused by the soil pressure difference.

I. Introduction

It is a well known fact that there is a certain ascending electric current on the surface of a slope of the earth.

The writer measured the distributions of the potential gradient of the earth current on the two cinder cones of Kome-tsuka and Ôgi-yama which are extinct volcanoes. He also made similar measurements on other volcanic cones, such as the Ôjo-dake and the Yomine. Having investigated the distributions of the potential gradient of the earth current, he found that;

1). In the case of cinder cones, they were caused by the pressure of the earth.

2). In the case of conides, the distributions of the potential gradient caused by the pressure of the earth were disturbed by the lava flow.

II. The Instrument and Method of Measurements

§ 1. *Potentiometer.* P. P. P. type portable potentiometer, manufactured by the Shimazu Manufacturing Co., is used; its whole resistance is 950 ohms, sensibility is one m. v. And by means of this potentiometer it is possible to measure from 0.1 m. v. to 1.4 volts.

§ 2. *Pole Pieces.* A Cu pole 6 mm × 20 cm is cut equally in two, one of these pieces being used as positive pole and the other as negative. Each of these two pieces of the Cu pole is inserted into an unglazed porcelain pot (2 cm × 15 cm) which has been filled with pow-

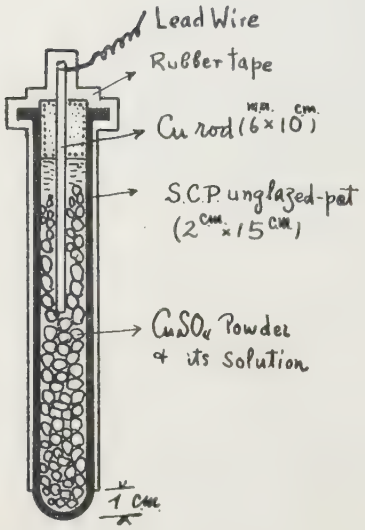

Fig. 1. Section of a Pole Piece.

dered chemically pure $CuSO_4$ crystal and water. Then these pots are sealed with rubber corks. They should not be filled up to the lower part of the cork with $CuSO_4$ powder, but space of several millimeters must be left for water only so that the content of the pot may be mingled.

The outside of the pot is taped with rubber tape that it may be well insulated and also kept warm, but the lower one centimeter of it must be left untaped so that that portion may make contact with the soil. When these pots are not in use, the portion of contact should be wet with a wet sponge. A set which the writer is now using have the fixed voltage of 1.8 m. v. This may be due to the impurity of the content of the unglazed porcelain. In this field measurement, this fixed voltage has shown no change.

§ 3. *Manipulation.* The potentiometer set described is very convenient to handle so that we have been able to observe the main current promptly at any time desired during the measurement. The distance between the poles is 50 meters and the poles are connected with rubber cord (s. w. g. 20) 60 meters in length. After the reading is made, the poles are exchanged and the reading is made again. After taking the mean value of the two, the fixed voltage of the pole piece is subtracted.

In the readings 0.1 m. v. has been adopted, but with the consideration of several questions at the time of the field work, it is desired to adopt up to 10 m. v. The pole pieces are inserted into the soil for 20 cm.

III. Results of Measurements

§ 4. *The Cinder Cone "Kome-tsuka".* There is a cinder cone 954 meters above the sea level at the foot of the north-west of Kishima-dake, one of Aso's five central cones. It is called Kome-tsuka (Fig. 2A). The whole cone is covered with grass. It has the shape of a truncated cone and rises about 50 meters above the level ground. The crater at the

top of the cone is about 10 meters deep and 100 meters in diameter. We took the middle of the crater as the center (origin), covering the whole hill with observation points forming a net whose sides are 50 meters long, and measured the direction of the potential gradient of the earth current. We found that the currents gather on the north top of the crater rim as is shown in Fig. 2 C. It agrees with the report of J. E. Burbank that "Earth currents are known to flow from all sides up a mountain toward the top".*

It was found that Kome-tsuka has an almost homogeneous structure under the part of the mountain we surveyed. This will be shown later in the present paper. At the time of the survey, we found no considerable difference in the temperature between the top and the foot of the mountain (Table 1).

Table 1. Temperatures at the Kome-tsuka. (1936 June 7th)

Center	22.2°C
North foot	23.0°C
West foot	22.6°C
South foot	23.0°C
East foot	22.3°C

(each at the surface)

The equation of the profile of this volcano is calculated as $y = 11\varepsilon^{0.01x}$ from the observation data (Table 2). In the equation the origin is at the top of the cone, x means the horizontal distance, and y means the vertical downward distance from the origin.

Table 2. Observed difference of the points.
(Kome-tsuka, 1936 June 7th)

Points	(O, O ; O, E_1)	(O, E_1 ; O, E_2)	(O, E_2 ; O, E_3)
	←	→	→
Height Diff.	15.95m	16.25	25.60
Potent. Diff.	4.8mv	74.8	81.7
	←	←	←
Points	(O, O; O, N_1)	(O, N_1 ; O, N_2)	(O, N_2 ; O, N_3)
	←	→	→
Height Diff.	11.90m	22.05	25.10
Potent. Diff.	42.7mv	38.3	34.0
	→	←	←
Points	(O, O; O, W_1)	(O, W_1 ; O, W_2)	(O, W_2 ; O, W_3)
	←	→	→
Height Diff.	12.50m	22.45	27.60
Potent. Diff.	36.9mV	98.3	46.8
	→	←	←

* J. E. Burbank :– Earth-currents and a proposed method for their investigation. Terr. Magn. and Atmos. Electr. Vol. 10. 1905. pp. 23-49.

Points	(O, O; O, S_1)	(O, S_1; O, S_1)	(O, S_2; O, S_3)
Height Diff.	6.60m	21.15	26.40
Potent. Diff.	19.0mv	101.4	46.3
Points	(O, N_1; E_1, N_1)	(E_1, N_1; E_2, N_1)	(E_2, N_1; E_3, N_1)
Height Diff.	1.95m	17.75	24.85
Potent. Diff.	15.0mv	77.1	71.0
Points	(O, N_1; W_1, N_1)	(W_1, N_1; W_2, N_1)	(W_2, N_1; W_3, N_2)
Height Diff.	5.45m	17.75	24.85
Potent. Diff.	38.8mv	49.0	56.0
Points	(O, S_1; E_1, S_1)	(E_1, S_1; E_2, S_1)	(E_2, S_1; E_3, S_1)
Height Diff.	3.05m	17.40	21.20
Potent. Diff.	41.5mv	68.8	52.3
Points	(O, S_1; W_1, S_1)	(W_1, S_1; W_2, S_1)	(W_2, S_1; W_3, S_1)
Height Diff.	6.00m	22.55	26.10
Potent. Diff.	48.1mv	68.0	31.5
Points	(O, E_1; E_1, N_1)	(E_1, N_1; E_1, N_2)	(E_1, N_2; E_1, N_3)
Height Diff.	5.50m	16.18	23.75
Potent. Diff.	3.5mv	28.7	23.5
Points	(O, W_1; W_1, N_1)	(W_1, N_1; W_1, N_2)	(W_1, N_2; W_1, N_3)
Height Diff.	7.25m	20.90	25.80
Potent. Diff.	24.0mv	33.7	24.4
Points	(O, E_1; E_1, S_2)	(E_1, S_1; E_1, S_2)	(E_1, S_2; E_1, S_3)
Height Diff.	11.45m	25.20	27.50
Potent. Diff.	65.0mv	78.0	50.5
Points	(O, W_1; W_1, S_1)	(W_1, S_1; S_1, W_2)	(W_1, S_2; W_1, S_3)
Height Diff.	13.00m	23.00	25.50
Potent. Diff.	107.3mv	70.0	33.9

Points	(O, O; 1)	(1; 2)	(2; 3)
Mean Height Diff.	3.74m	20.17m	25.16m
Mean Potent. Diff.	27.2mv	62.6mv	44.4mv

From the above data we can find the co-ordinates of the points as:—

Points . . . . . (top), (1), (2), (3).

x, y . . . . . (0, 0), (50, 4), (96, 24), (139, 49).

The graph in Fig. 2B shows the mean values of measurement of po-

Fig. 2 A

Kome-tsuka (The View from South).

Fig. 2 B

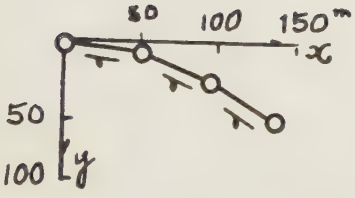

Mean Profile of the Cone.
(Kome-tsuka)

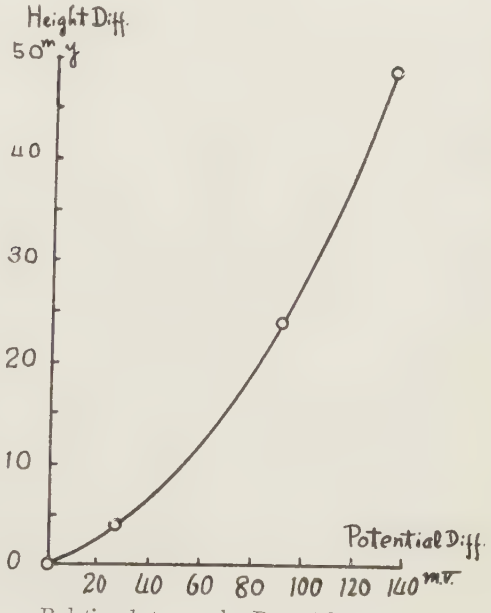

Relation between the Potential Difference
and the Height Difference. (Kome-tsuka)

Fig. 2 C

High○→○Low (Kome-tsuka)

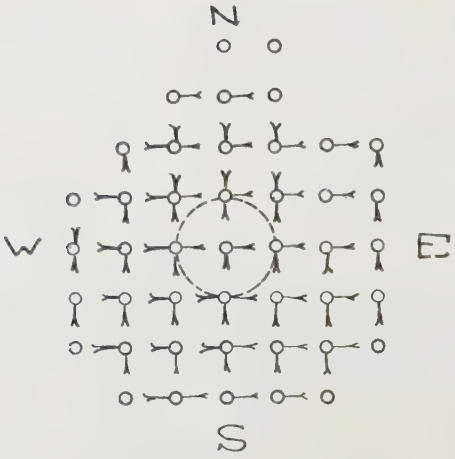

Height Differences of the Points.

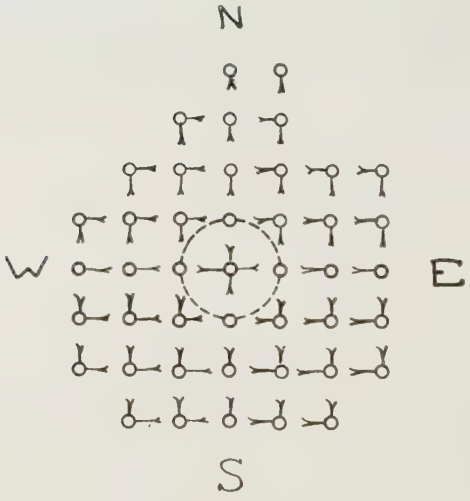

Potential Differences of them.

tential gradient of the earth current at each point and its height differences. This is not a straight line, but a perfect curve which is rather concave toward the y axis (the height difference axis).

§ 5. *The Cinder Cone "Ôgi-yama"*. The Ôgi-yama volcano, 792.0 meters above the sea, is a cinder cone whose skirt extends toward Beppu Bay. The east and west sides are somewhat flat, and the slope develops on the north and south sides. The differences of the height and potential differences measured along the south-north line are indicated in Table 3.

This is illustrated in Fig. 3.

Table 3. Data at Ôgi-yama.
(1936 Aug. 17th.)

Points (North)	(Top ; 1)	(1 ; 2)	(2 ; 3)	(3 ; 4)	(4 ; 5)	(5 ; 6)	(6 ; 7)
Height Diff.	10.57^{m} →	19.69 →	20.02 →	20.89 →	19.37 →	20.57 →	19.15 →
Potential Diff.	11.19^{mv} →	50.7 →	2.0 →	44.5 ←	123.4 ←	108.9 ←	128.8 ←

Points (South)	(Top ; 1)	(1 ; 2)	(2 ; 3)	(3 ; 4)	(4 ; 5)	(5 ; 6)
Height Diff.	→ 21.32m	→ 23.50	→ 26.19	→ 23.16	→ 16.68	→ 19.30
Potential Diff.	← 197.0mv	← 203.0	← 127.0	← 148.2	← 226.0	← 115.5

Points	(Top ; 1)	(1 ; 2)	(2 ; 3)	(3 ; 4)	(4 ; 5)	(5 ; 6)	(6 ; 7)
Mean H. D.	→ 15.95m	→ 21.60	→ 23.11	→ 22.03	→ 18.03	→ 19.94	→ 19.15
Mean P. D.	42.6mv ←	76.2 ←	62.5 ←	96.4 ←	174.7 ←	112.2 ←	128.8 ←

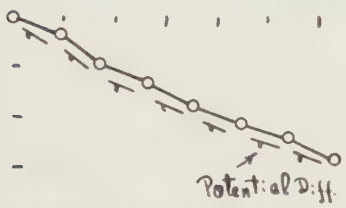

Fig. 3. Profile of the Cone. (Ôgi-yama)

§ 6. *The Toloide "Yomine"*. This is the oldest volcano, 913 meters above the sea, among the group of the volcanic central cones of Mt. Aso; its slopes extend to the east, south, and the west sides of the mountain, while the northern slope faces the blasted crater of the Jigoku and it is covered with the lava of the Eboshi-dake. The northern slope is planted with trees, while three other sides are covered with grass.

The relation of the height and the potential differences measured along EW line is shown in the table 4 and Fig. 4.

Table 4. Data at Yomine.
(1936 Aug. 11th.)

Points	(Top-1)	(1-2)	(2-3)	(3-4)	(4-5)	(5-6)	(6-7)	(7-8)	……East
H. D.	→ 4.03m	→ 8.91	→ 11.02	→ 11.08	→ 12.21	→ 15.02	→ 20.20	→ 26.45	
P. D.	← 17.3mv	← 42.4	← 15.8	← 12.3	← 3.3	→ 0.3	→ 9.0	→ 3.0	
H. D.	→ 3.88m	→ 4.55	→ 6.62	→ 15.55	→ 23.74	→ 26.00	→ 26.82	→ 26.50	……West
P. D.	→ 35.0mv	→ 10.0	→ 14.0	→ 9.6	← 26.5	← 27.5	← 37.6	← 50.5	
H. D.	→ 18.75m	→ 20.60	→ 20.10	→ 28.95	→ 20.30	→ 28.70	→ 20.70	→ 31.65	……South
P. D.	← 26.7mv	← 8.4	→ 3.0	→ 11.0	→ 6.4	→ 9.0	→ 2.0	→ 44.5	

The Mean Values in EW line								
H. D.	→ 3.96m	→ 6.73	→ 8.82	→ 13.32	→ 17.98	→ 20.51	→ 28.01	→ 26.48
P. D.	→ 8.9mv	← 16.2	← 0.9	← 1.9	← 11.6	← 13.6	← 14.3	← 23.8

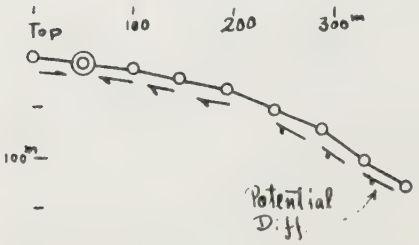

Fig. 4. Profile of the Cone. (Yomine)

And the graph of the measurement above mentioned is entirely different, taking the measurement southward from the triangle point into consideration, from those of Kome-tsuka and Ôgi-yama, and here we find there are potential differences which face downward from the top. This seems to me to show that there is a lava flow under the ground. If we examine the graph on the differences of height and potential, it is noticeable that the direction of the potential gradients from the foot and the top comes together about 50 meters from the top. This may be the effect of the under ground lava flow (Aug. Hype. andesite) which exists near that level.

§ 7. *The Conide Ôjo-dake.* Ôjo-dake is one of the Aso central cones and it is the same mountain that is recorded as Kishima-dake in the history of Higo-Kokushi and also in the report No. 33 of the Japan Earthquake Inv. Committee. Its height is 1238.1 meters according to our Land Survey map. There are three craters on this mountain. The northern rim of the western crater and its northern slope develop on the lave flow which covers the western half of Aso-dani. This

Table 5. Data at the Conide Ôjo-dake.
(1936 Sept. 1st.)

Points (North)	(Δ-1)	(1-2)	(2 3)	(3-4)	(4-5)	(5-6)	(6-7)	(7-8)	(8-9)	(9-10)
H. D.	→ 15.15m	→ 21.00	→ 23.75	→ 47.60		→ 24.55	→ 18.70	→ 20.60	→ 23.85	→ 19.70
P. D.	→ 78.5mv	→ 50.0	→ 54.5	→ 46.5	→ 10.9	← 5.1	← 18.8	← 9.6	→ 29.0	→ 23.5

	(10-11)	(11-12)	(12 13)	(13-14)	(14-15)	(15-16)	(16-17)
	→ 29.70m	→ 19.95	→ 19.20	→ 11.50	→ 8.25	→ 10.50	→ 15.20
	→ 6.0mv	← 13.0	← 41.0	← 32.5	← 17.0	← 12.5	← 3.0

volcano commands a very beautiful scene of pasture land, and it is determined as the conide.

As the distribution of the potential differences of the earth current can be measured only on the northern half, we cannot form any definite conclusion, but in general we can make it clear. Data are in the table 5 and the relation graph is in Fig. 5.

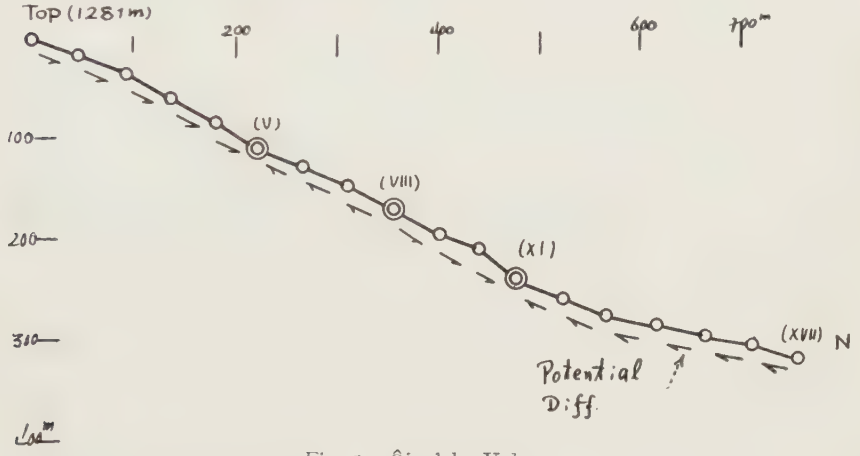

Fig. 5. Ôjo-dake Volcano.

§ 8. *The Ground of the Aso-Volcanic-Laboratory.* This ground is a layer of loam about 20 meters thick on the top of a mound-like hill which was made at the time of the first lava flow of the Eboshi-

Table 6. Data at the ground of the Aso-Volcanic-Laboratory.
(1936 May 20th.)

Points	(Top-1)	(1-2)	(2-3)	(3-4)	
H. D.	→6.42m	→18.32	→18.33		.....North
P. D.	→52.5mv	→1.1			
H. D.	→0.33m	→8.80	→9.31	→11.49	.....South
P. D.	→100.8mv	→1.1	←25.8	←28.8	
H. D.	→0.05m	→6.19	→3.21	→11.07	.....East
P. D.	→14.3mv	→4.30	←1.5		
H. D.	→8.00m	→15.94	→14.72	→10.48	.....West
P. D.	→30.4mv	0.0	←25.0		
Mean Values H. D.	→3.9m	→12.31	→11.49	→11.01	
P. D.	→49.5mv	→11.3	←17.8		

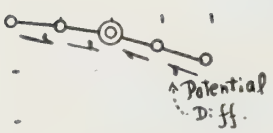

Fig. 6. Profile of Kenkyu-Sho-Yama.

dake. On the top of this hill (567.7 meters high), is the main building of the volcanic laboratory, a steel concrete structure about 40 m × 40 m. The ground is covered with grass only. The distributions of the earth current are very complicated as shown in table 6 and Fig. 6.

§ 9. *The Adjustment of the Observations.*

1). In general, the meeting point of the rising current and the falling current is at the west and north sides of the mountain top, and in the mean curve it disappears. This may show that the general current of the neighbouring earth current lies in this direction. Consequently, we can infer the direction of the earth current in that vicinity from the place of this changing point.

We arranged the observation points in symmetry on the other side of the mountain top, because we wanted to find only the distributions of potential. The general current of the field was eliminated.

2). As there is generally considerable thick loam on the mountain top, if there were no obstacles such as forests or buildings, we should have had sufficient results indicating the potential distributions in the direction which corresponds to the direction of the general earth current, at the top of any mountain of the cinder, toloide, and conide.

3). On the toloide, the conide and the lava flow, the potential caused by height differences is influenced and so the observed potential gradient of the earth current is very complicated.

4). The temperatures of the earth's surface at various observation points are not very different.

Table 7. Temperatures at the observation points.

Kome-tsuka	Top	22.2°C (Surface)
	North foot	23.0°
	South	23.0°
	East	22.3°
	West	22.6°
Ôgi-yama	Top	18.0°C
	South	18.0°
	North	18.0°
Yomine	Top	18.0°C
	East foot	17.5
	West	18.0
	South	18.0
Ôjo-dake	Top	17.5°C
	North	17.0

Volcanic Laboratory =	Top	17.5°C
	East foot	17.3
	West „	18.0
	North „	17.8
	South „	18.0

5). In spite of this, if we examine the height differences and the potential gradient of the earth current on a cinder cone, it may show comparatively smooth relation curves.

Inferring from the results above, I think that the cinder cone has a comparatively uniform structure, and the ascending electric current toward the mountain top is caused by the height differences, namely, the differences of the soil pressures or the differences of some other amount which changes parallel to the differences of soil pressure.

IV. The Relation between the Height Differences and the Potential Differences of the Earth Current

In connection with the nature of the potential difference observed above, the writer put the freshly dug soil (from about 10 cm. underground) into a bamboo tube of 11 cm. in inner diameter and 130 cm. in length, and buried the two poles and made the distance of the pole pieces to be 100 cm. The pole piece is an amalgamated zinc rod 1 cm. in diameter and 2 cm. in length as shown in Fig. 7. And then we

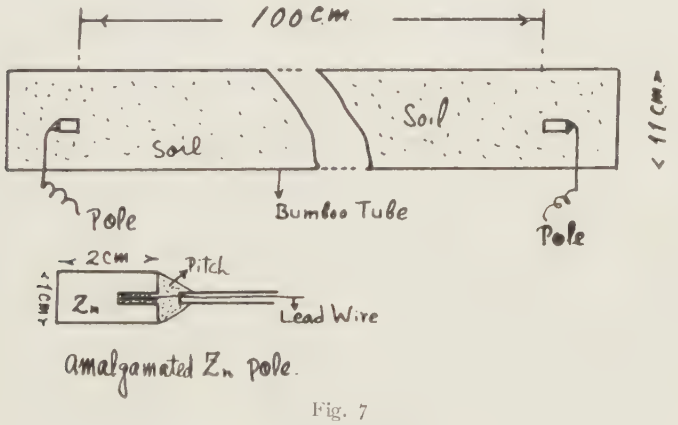

Fig. 7

stuffed the rubber cord with the zinc piece into the hole of the rod, and insulated the cord thoroughly with pitch. Both ends of the tube are insulated with rubber boards and once more fixed with wooden pieces. At the time of experiment, we increased or decreased the

voltage differences between the poles, fixing one end and making the bamboo tube diagonal by moving the other end. After the preparations were made, we placed the bamboo tube level, and left it about 48 hours, keeping the temperature uniform.

For the measurement of potential differences we used the potentiometer of Leed and Northrup Co. and were able to read to 10^{-3} m. v. by the balance method.

Table 8. Potential Differences of a Soil Column under various Heights. (moderate moisture)

Time	Height Diff.	Voltage gained 1936 Sept. 28th.			
10h25m	20cm	+0.000233volt	12h40m	20cm	+0.000149volt
35	40	396	50	40	375
45	60	573	13 0	60	523
55	80	662	10	80	684
11 05	100	839	20	100	882
11h40m	20cm	+0.000226volt			
50	40	329		20cm	+0.000208volt
12 0	60	524	Mean Values	40	+ 368
10	80	702		60	+ 540
12 20	100	870		80	+ 682
				100	+ 864

Table 9. Potential Difference of a Soil Column under various Heights. (excessive moisture)

Time	Height Diff.	Voltage gained 1936 Sept. 25th.			
11h10m	20cm	−0.000165volt	15h20m	20cm	−0.000158volt
12 10	40	− 269	25	40	− 293
13 10	60	− 365	30	60	− 436
14 10	80	− 646	35	80	− 502
15 10	100	− 833	40	100	− 634
	20cm	−0.000162volt			
	40	− 281			
Mean Value	60	− 401	*Notice*		
	80	− 574	+Lower pole.....positive		
	100	− 734	−Lower pole.....negative		

Readings :—

1). First of all, we read the potential differences in the horizontal position.

2). Then one end was raised so that the height differences between the two poles became the desired value and another reading taken.

3). Again the tube was brought back to the level position, and a reading taken.

We finished this process within three minutes, and left it ten minutes as it was, and then measured at the next position. This result is shown in tables 8 and 9, Figs. 8 and 9.

This result agrees with the reports made by S. J. Mauchly* that the lower pole becomes positive potential when the soil is moistened moderately, and it becomes negative when the soil is excessively moist. And I found out that the height difference and the potential differences were in linear relation as shown in the figure.

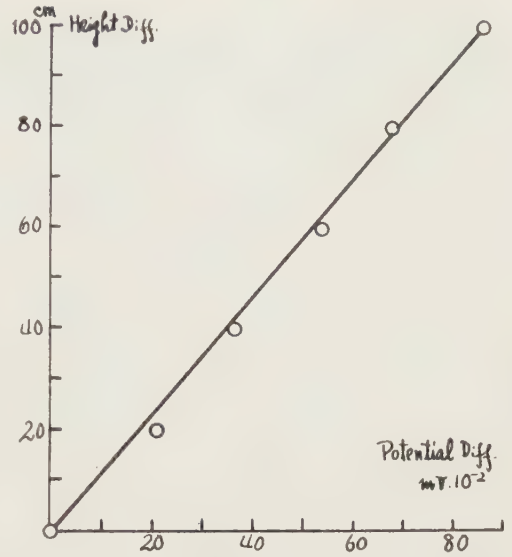

Fig. 8. Potential Differences of a Soil Column under various Pressures. (moderate moisture)

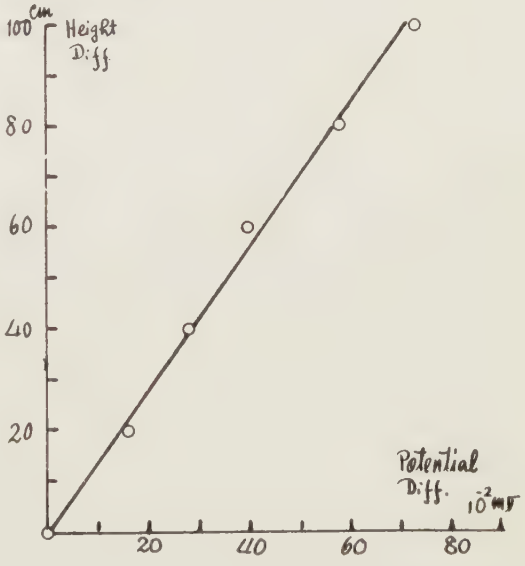

Fig. 9. Potential Differences of a Soil Column under various Pressures. (saturated moisture)

* S. J. Mauchly :— A study of pressure and temperature effects in earth current measurements. Terr. Magn. and Atm. Electr. **23**, 1918, pp. 73-91.

Moreover, I noticed that the potential differences caused by the pressure differences were due to the phenomenon of the streaming potential. As in Mauchly's observation, the phenomenon that the upper pole becomes positive when the moisture is in excess, that is, the phenomenon making the ascending current disappear when the cataphoresis becomes vigorous, is the same with the phenomenon in the electrolyzable solution. On the contrary, the lower pole becomes positive in moderate moisture, the ascending current becomes stronger, and the cataphoresis weaker.

From these experiments, we may infer that it is the phenomenon of the streaming potential to produce the potential differences by the height differences of the soil column. Again briefly, when there is an excessive moisture, the colloidal particles are pressed down, and the so-called cataphoresis is produced; and in less moisture, the water is pressed down, and the so-called streaming potential is produced. And the potential differences generated in that case, using the result of Helmholtz, are as follows:—

$$E=\frac{P.D.\zeta}{4\pi.\eta.\lambda}$$ where

E: Potential gained.
P: Pressure.
D: Dielectric constant.
ζ: Potential of the double layer.
η: Coefficient of viscosity of the water.
λ: Specific conductivity of the soil.

In fact, the phenomenon of excessive moisture in the soil of the volcanic districts seldom happens and so the lower pole is usually positive on the surface of the earth.

Now the distribution of the "boden druck" under a "grundungs körper" is in general:

$$P=P_0\cdot\left(1-\frac{x^2}{a^2}-\frac{y^2}{b^2}\right)^m$$ where

$m>1$
$P(x,y)$: boden druck at (xy),
P_0: boden druck at the center,
$a,\ b$: constants.

As it is used in general,

$$P=P_0\cdot\left(1-\frac{x^2}{a^2}\right)$$ where $m=1$, and x, y are in symmetry,

then the boden druck $=\Pi\cdot\int_0^{P_0}x^2dP$.

Therefore $$P_0=\frac{2}{\Pi\cdot a^2}\text{(total boden druck)}.$$

The volcanic cone is not a uniform "grundungs körper" as in the above case, but if the mean pressures are distributed at each horizontal surface, the pressure P_0 at the center becomes as follows :—

Let the equation of the cone be $y=a\cdot e^{c_1x+c_2x^2+\cdots\cdots}$, $c>0$ and $y=a\cdot e^{cx}$

then $$P_0=\frac{2\cdot\rho\cdot g}{x^2}\int_a^y x^2\cdot dy$$

$$=2\cdot\rho\cdot g\cdot\left[y-2\cdot y\cdot\log^{-1}\frac{y}{a}+2(y-a)\log^{-2}\frac{y}{a}\right]$$

where ρ=density, g=980 cm/sec./sec.

This is concave toward the y axis when y is nearly equal to a, and becomes more concave toward the P axis when y is fairly large. If the potential gradient which was measured at the side of the cinder cone is caused by the difference of the maximum pressure P_0 on that level surface, it will be represented by the following equation :

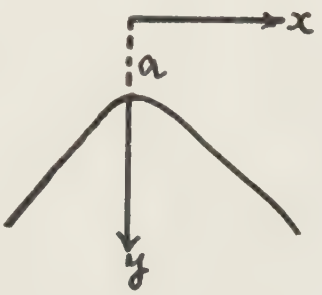

Fig. 10

Potential difference=function (P_0)

$$=a\cdot\left(y-\frac{2y}{\log y-\log a}+\frac{2(y-a)}{(\log y-\log a)^2}\right).$$

If the ascending current of the earth current which appears in a cinder cone which is comparatively not very high, may be mainly due as above to P_0, the potential difference must be a function of P_0 and, therefore, be a function of the altitude difference. Moreover if the potential differences caused by the height differences depend on the streaming potential, the specific conductivity, the dielectric constant and the viscidity of the water of each volcano play very important parts as shown in the equation. We found that the theoretical equation coincided with the result of the field observation on these points. That is to say that the ascending current which appears in a cinder cone comparatively not very high, may be mainly due to the streaming potential which is produced by the difference of the soil pressure in the altitude difference. If we use the result in reversal, it is possible to find out a cone to be either a cinder one or not.

In conclusion the author wishes to express his sincere thanks to Prof. T. Nomitsu for his kind advice and encouragement during the study.

On the Densities of Various Fibres and the Widths of the Intermicellar Spaces

By **Yoshiaki Matsunaga**

(Received October 5, 1938)

Abstract

Intermicellar spaces of various textile fibres were examined by measuring their densities and their swellings in water, in various primary normal alcohols, and in liquid paraffin. It was observed that the density of a fibre which was measured in methyl alcohol was greater than those measured in the other liquids, and that the density decreased with the number of carbon atoms of the alcohols and the liquid paraffin.

Introduction

The density of a fibre has frequently been measured in water. But according to the recent research made by the writer[1] the water molecules penetrate, as molecular groups, into the intermicellar space of the fibre which is constructed with the micellar structure. And the water molecules, even when the fibre is swollen perfectly in it, cannot completely penetrate into the intermicellar space. This means that the density of the fibre measured in water may be considered as giving an apparent density somewhat smaller than its net density. Thus the density of the fibre measured in methyl alcohol, the chain length of whose molecules are short, is greater than that measured in water, as has already been reported in connection with silk and ramie.

According to G. W. Stewart and R. M. Morrow,[2] the lateral thickness of the molecules of the primary normal alcohols is considered to be approximately constant, and their chain length increases with the number of the carbon atoms.

When the density of the fibre is measured in various primary normal alcohols, the molecules of the alcohols penetrate into the intermicellar space to different degrees according to the chain length of the alcoholic molecules. Consequently the variation of the densities measured in various primary normal alcohols shows the proportion of the intermicellar spaces having different widths.

1. Y. Matsunaga: These Memoirs, **20**, 157 (1937).
2. G. W. Stewart & R. M. Morrow: Phys. Rev., **30**, 232 (1927).

In the present investigation the writer measured the density of wool, silk, reworked silk, ramie, cotton wool, and viscose rayon in water, in various primary normal alcohols and in liquid paraffin by the evacuation method employed by U. Yoshida and B. Takei,[1] which is especially suitable for obtaining the net densities of porous and powdery substances; and at the same time the mean lateral swelling of the fibres in the above mentioned liquids were measured.

Consideration from the Density

The densities of wool, silk, reworked silk, ramie, cotton wool, and viscose rayon were measured in water, in primary normal alcohols from methyl to amyl and in liquid paraffin by the evacuation method devised by U. Yoshida and B. Takei. The results are tabulated in Table I, and are shown in Figs. from 1 to 6.

Table I

	Wool	Silk (Fibroin)	Reworked silk	Ramie	Cotton wool	Viscose rayon
Water	1.399	1.426	1.425	1.614	1.604	1.614
Methyl alcohol	1.410	1.483	1.440	1.629	1.641	1.614
Ethyl alcohol	1.404	1.445	1.409	1.591	1.637	1.580
n. Propyl alcohol	1.372	1.382	1.361	1.589	1.597	1.580
n. Butyl alcohol	1.367	1.380	1.364	1.584	1.597	1.563
n. Amyl alcohol	1.366	1.382	1.366	1.580	1.600	1.550
Liquid paraffin	1.322	1.363	1.329	1.519	1.558	1.522

Fig. 1
Wool

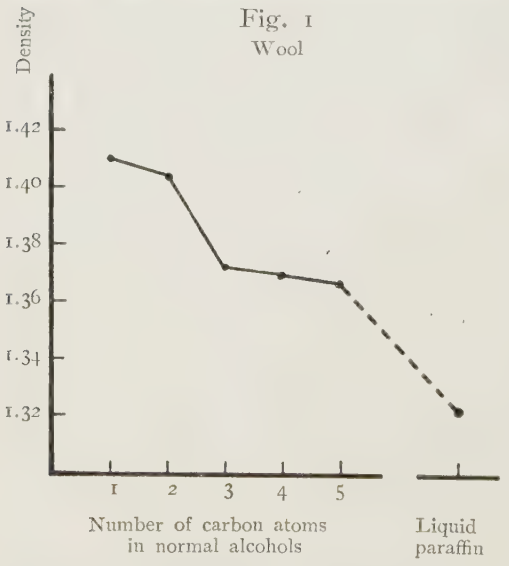

As will be seen in the Table, and by the figures the densities of these fibres, except viscose rayon, are greater in methyl alcohol than when measured in water and they decrease with the size of the mole-

1. U. Yoshida & B. Takei: These Memoirs, **15**, 1 (1932).

Fig. 2

Silk

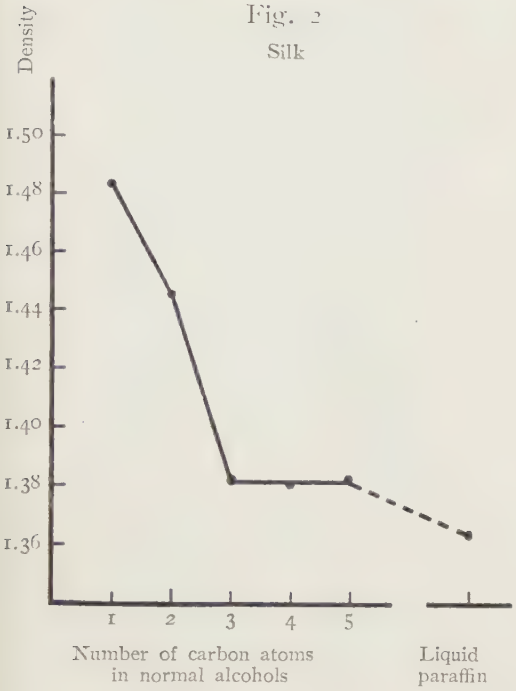

Fig. 4

Ramie

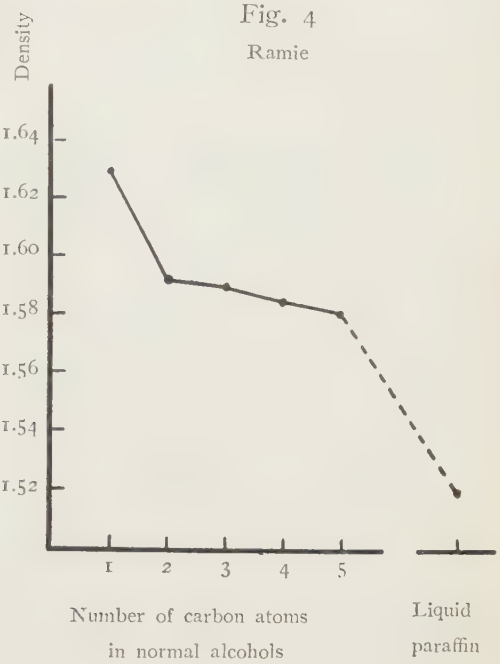

Fig. 3

Reworked silk

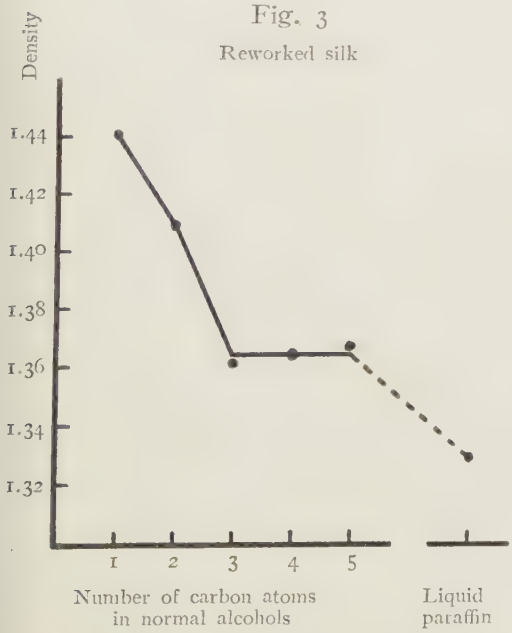

Fig. 5

Cotton wool

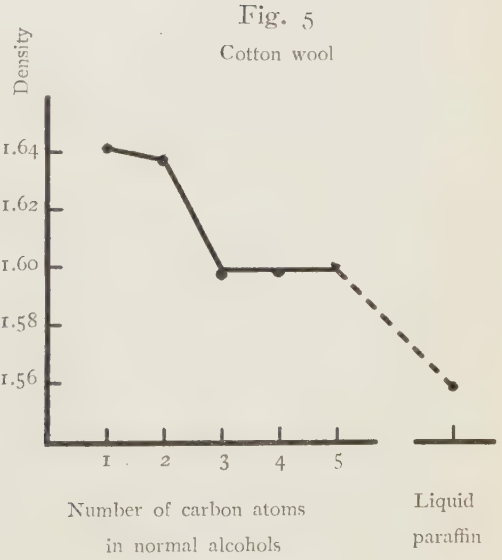

Fig. 6

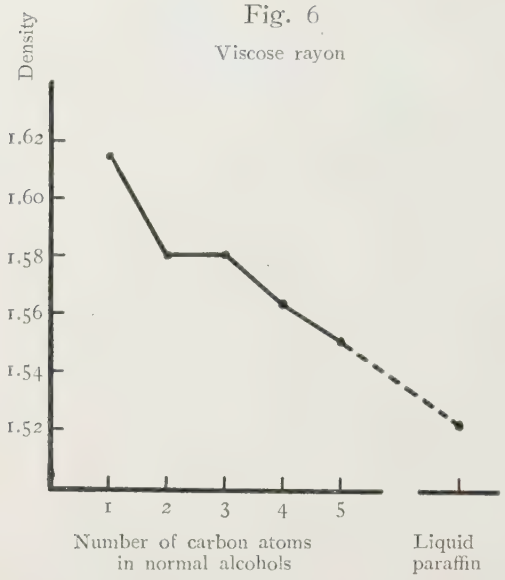

cules of various kinds of alcohols; but the density of viscose rayon is the same in methyl alcohol as in water and decreases with the size of the molecules of various kinds of alcohol.

A thorough investigation with the X-ray diffraction of the primary normal alcohols from methyl to lauryl, has already been carried out by G. W. Stewart and R. M. Morrow.[1] Each alcohol gave rise to two diffraction peaks. One of these peaks was practically independent of the carbon content of the alcohol and appeared to be associated with the lateral thickness of the molecule. The other is associated with the chain length and gives an increase of 1.3 A. U. per one carbon atom. Next B. E. Warren[2] has given a more correct interpretation of the inner peaks observed with alcohols and fatty acids. The corrected lengths of the chain of primary normal alcohols are tabulated in Table II.

Table II

Number of carbon atoms	Length of chain in A. U.
1	4.3
2	5.7
3	6.9
4	7.9
5	9.0

The normal paraffins were studied by C. H. Sogani[3] and G. W. Stewart.[4] The formula proposed by Stewart for their chain length L is

$$L=\frac{\text{Molecular weight}\times\text{Mass of H atom}}{(4.64\times10^{-8})^2\times\text{Density}}.$$

When the values L obtained from the above relation are plotted against the number n of the carbon atoms in the chain molecules of the

1. G. W. Stewart & R. M. Morrow: *loc. cit.*
2. B. E. Warren: Phy. Rev., **44**, 969 (1933).
3. C. H. Sogani: Indian J. Phys., **2**, 97 (1928).
4. G. W. Stewart: Phys. Rev., **31**, 174 (1928) & **32**, 153 (1928).

paraffins, it is found that the above formula is reduced to the following linear relation:

$$L = 1.24\,n + 2.70.$$

Thus the distance 1.24 A. U. represents the distance between two adjacent carbon atoms. By assuming as is reasonable, that the liquid paraffin used in the present experiment consists only of normal paraffins, the number of the carbon atoms is estimated to be 10–15; which give the values of 15–20 A. U. to the chain lengths of the paraffin molecules by the above formula.

The reason why the densities of the fibres decrease with the length of the molecular chain of the alcohols and liquid paraffin seems to be the increasing difficulty of penetrating into the narrow intermicellar space of the fibres with increasing chain lengths of the molecules.

Consideration on the Intermicellar Space

In Figs. from 1 to 6, the densities of the fibres are taken as the ordinates and the number of the carbon atoms of various alcohols and liquid paraffin are taken as abscissae. As is evident from the curves in these figures, the density of every fibre decreases at first as the number of the carbon atoms of the alcohols increases, then it becomes constant for a few of the following carbon atoms, and lastly it decreases again with the increasing number of the carbon atoms. This behaviour of the density of the fibres is due to the uneven proportion of the intermicellar spaces having different widths. The fact that the density of a fibre is constant for a time in alcohols containing a successively increasing number of carbon atoms indicates that the volume of the intermicellar spaces of a fibre into which the molecules of these alcohols can and cannot penetrate are respectively the same for all of these alcohols.

Consequently it may be inferred that the intermicellar spaces having a range of widths somewhat narrower than the chain lengths of these alcohols are missing. Thus the intermicellar spaces of a fibre may be said to consist of two parts: one which is narrower than and the other which is wider than

Fig. 7

Approximate curve for silk

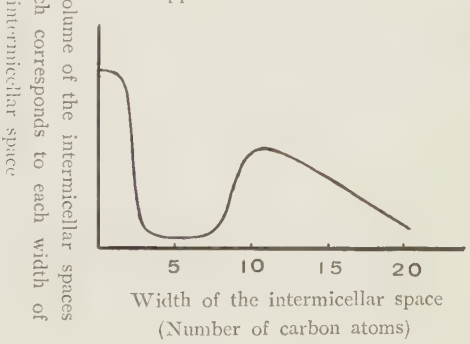

the missing portion. The proportion of the volume of the intermicellar spaces having different widths is shown schematically by the curve in Fig. 7 for the case of silk as an example.

In the case of wool fibre, silk fibre, reworked silk fibre and cotton wool fibre the first intermicellar space is narrower than the chain length of the molecule of propyl alcohol, and the second one is wider than the chain length of the molecule of amyl alcohol. In the cace of ramie fibre, the first intermicellar space is narrower than the chain length of the molecule of ethyl alcohol and the second one is wider than the chain length of the molecule of amyl alcohol. Lastly in the case of viscose rayon the first intermicellar space is narrower than the chain length of the molecule of ethyl alcohol and the second one is wider than the chain length of the molecule of propyl alcohol.

N. Matsumoto[1] estimated the width of the intermicellar space of viscose rayon by means of X-ray patterns. The specimen was at first immersed in a solution of about 0.5% $HAuCl_4$, and then the $HAuCl_4$ in the fibre was reduced to Au in the vapour of Hydrazine Hydrate. The size of the microcrystals of Au thus deposited in the intermicellar space of the fibre was estimated from the microphotometer curve of Debye-Scherrer X-ray patterns, and he concluded, from the size of Au-crystals thus estimated, that the mean width of the intermicellar space of viscose rayon is 65–69 A. U. Recently Frey-Wissling[2] measured, by the same method, the widths of the intermicellar space of various fibres. The results are as follows: natural cellulose 85–135 A. U., acetyl cellulose 60 A. U., viscose rayon 50 A. U., silk fibre 50 A. U. and wool fibre 60 A. U.

On the other hand Y. Hiratsuka and J. Hori[3] estimated the width of the intermicellar space of ramie fibre as 17–16 A. U., by assuming that the volume of water which was adsorbed from the perfectly dry state to the normal state is equal to the total volume of the intermicellar spaces, and also that the size of the micell is $200 \times 200 \times 500$ $(A. U.)^3$ or $200 \times 200 \times 1000$ $(A. U.)^3$.

More recently S. Iwasaki and T. Miyamoto[4] investigated the serigraph curve of viscose rayon immersed in paraffins, in normal al-

1. N. Matsumoto: Soc. Chem. Industry Japan, **37**, 827 (1934).
2. Frey-Wissling: Protoplasma, **27**, 372 (1937).
3. Y. Hiratsuka & J. Hori: Oyo Butsuri, **4**, 9 (1935).
4. S. Iwasaki & T. Miyamoto: Soc. Chem. Industry Japan, **41**, 440 (1938).

cohols, and in normal fatty acids; and concluded that two kinds of intermicellar spaces exist, having different widths.

Thus the widths of the intermicellar spaces of the fibres are different according to the methods of measurement. This seems to indicate that the intermicellar spaces of a fibre are not uniform, but their widths extend unevenly over a pretty wide range in accordance with the present investigation, and that as the experimental method is different, different portions of the intermicellar spaces of different width are detected.

Next the writer measured with a microscope the lateral swellings of the fibres in water, in various primary normal alcohols, and in liquid paraffin. After the diameter of a fibre was measured in the air, the gases and water adsorbed by the fibre were taken off by evacuating with a Cenco Hyvac pump the glass tube containing the fibre at 100°C, and the glass tube was sealed. Then the glass tube was broken in water, in an alcohol or in liquid paraffin, and the diameter of the fibre was again measured after it had stood for 48 hours in it. The results are tabulated in Table III. The figures given in Table III refer to the ordinary state in air, which is swollen by a certain quantity of water. Therefore the positive sign indicates the expansion and the negative sign the contraction of the fibres in reference to the ordinary state in air.

Table III

Lateral swelling in % in reference to the ordinary state

	Wool	Silk (Fibroin)	Reworked silk	Ramie	Cotton wool	Viscose rayon
Water	+18.0	+19.7	+19.7	+13.0	+17.4	+31.5
Methyl alcohol	+ 3.8	+ 2.6	− 0.3	− 0.9	+ 4.4	+20.6
Ethyl alcohol	− 0.4	+ 3.8	− 0.5	+ 0.6	+ 3.8	+18.1
n. Propyl alcohol	+ 0.1	+ 2.6	− 2.6	+ 3.6	+ 3.4	− 2.7
n. Butyl alcohol	+ 1.6	+ 2.1	− 3.1	+ 0.6	+ 3.0	+ 0.2
n. Amyl alcohol	− 0.9	+ 1.6	− 3.0	− 0.2	+ 0.5	− 0.1
Liquid paraffin	− 0.9	− 3.1	− 4.1	− 5.2	− 1.8	− 4.8

Generally the lateral swelling of every kind of fibre is especially large in water, and in the alcohols and in liquid paraffin it is only a small expansion or contraction, less than a few per-cent, except with the viscose rayon in methyl and ethyl alcohols where the lateral swelling rises to about 20%. The prominent swelling in water seems to

be due to its surface tension which is remarkably strong as compared with that of the alcohols and the liquid paraffin; and the general tendency for the swelling to decrease with the number of carbon atoms in the alcohols and the liquid paraffin is probably caused by the increasing difficulty in penetrating into the narrow intermicellar spaces with the increasing chain length of the molecules.

Discussion

In Table III the figures of the lateral swellings of the fibres are respectively calculated in reference to the lateral dimensions of the fibres at an ordinary state. But under ordinary atmospheric conditions in Japan, namely a relative humidity of 70–80%, the fibres are already swollen to some extent as compared with the perfectly dry state.

The moisture thus adsorbed by the fibres at an ordinary state is taken off together with adsorbed gases by evacuation in measuring the lateral swelling; and a small contraction of the fibre will of course accompany this process. The apparent negative values of the lateral swelling as given in Table III have their origin in this fact; and the minimum diameters of the fibres measured in the liquid paraffin, corresponding respectively to the maximum apparent negative swellings, are taken approximately to be the same as those in the perfectly dry state.

Table IV shows the increase of the volume, expressed in per-cent, of the fibres swollen in various liquids in reference to their volume in liquid paraffin. Here it must be noted that the longitudinal swellings of the fibres are disregarded in calculating the increase of the volume by swelling since it is actually very small.

Table IV

Increase of volume by swelling in %

	Wool	Silk	Reworked silk	Ramie	Cotton wool	Viscose rayon
Water	41.8	52.5	55.8	42.1	43.0	86.9
Methyl alcohol	9.6	12.1	8.0	9.2	13.0	57.3
Ethyl alcohol	1.0	14.7	7.7	12.6	11.7	50.8
n. Propyl alcohol	2.0	12.1	3.2	19.5	10.9	2.2
n. Butyl alcohol	5.1	11.1	2.0	12.6	10.0	8.6
n. Amyl alcohol	0.0	9.8	2.2	10.9	4.7	7.7
Liquid paraffin	0.0	0.0	0.0	0.0	0.0	0.0

By substituting to s and $\frac{v}{V_1}$ the values given in Table IV and those obtained from equation (2), we get the values of $\frac{V_2''}{V_1}$ as given in Table V. In calculating thus the values of $\frac{V_2''}{V_1}$, we have assumed that the molecules of liquid paraffin cannot intrude into the intermicellar space of a fibre entirely. But this may not be so actually, and we can of course imagine the presence of still wider intermicellar spaces into which the molecules of the liquid paraffin can penetrate with ease. Consequently the values of $\frac{V_2''}{V_1}$ calculated in the above ought to be regarded as a minimum estimate.

Next the value of $\frac{V_2''}{V_1}$ can be checked by using the following relation :

$$\frac{V_2''-v'}{V_1 D}=x, \text{ i. e., } \frac{V_2''}{V_1}=xD+\frac{v'}{V_1}, \qquad (5)$$

where V_1, V_2'', v' and D denote the same meanings as before, and x the value of weight per-cent of the water adsorbed by a fibre in reference to the perfectly dried state when the fibre is put for 49 days in an enclosed space saturated with water vapour.

By putting in the equation (5), the value of the density of a fibre measured in methyl alcohol as D, the value of the water content x of a fibre which was measured by the writer and $\frac{v'}{V_1}$ as is given in Table VI for the case of water, we get the values of $\frac{V_2''}{V_1}$ as shown in Table VII. For the sake of comparison the values of $\frac{V_2''}{V_1}$ obtained from the expansion by swelling are tabulated in the last horizontal row of the table. Here it must be noticed that silk and reworked silk are omitted in the table as they are considered to swell in an intramicellar manner too. As is evident from Table VII, the values of $\frac{V_2''}{V_1}$ obtained by two different methods may be considered to be in rather good agreement, for such sort of experiments, though the discrepancy is a little more noticeable with viscose rayon than with the others. It has been stated before that the values of $\frac{V_2''}{V_1}$ obtained

Table VII

	Wool	Ramie	Cotton wool	Viscose rayon
D	1.410	1.629	1.641	1.614
x in weight per-cent	33.2	32	32	48.3
Dx	0.468	0.521	0.525	0.778
$\frac{v'}{V_1}$	0.008	0.009	0.023	0.000
$\frac{V_2''}{V_1}\left(=Dx+\frac{v'}{V_1}\right)$	0.48	0.53	0.55	0.78
$\frac{V_2''}{V_1}$ from Table V	0.513	0.523	0.506	0.981

from the expansion by swelling are a minimum estimate. But considering the fact that such minimum values agree respectively with those obtained from the increase of weight by swelling, the actual values of $\frac{V_2''}{V_1}$ seem to be well expressed by such a minimum estimate.

Next the writer examined how the lateral swellings of wool, silk, reworked silk, ramie, cotton wool, and viscose rayon in water proceed with time. The results are tabulated in Table VIII. The figures in Table VIII give the percentage of lateral swelling in reference to the diameter of the fibre in liquid paraffin, by considering the diameter of the fibre in it as approximately equal to that in vacuum, namely that of perfectly dried state.

Table VIII

Lateral swelling of fibre in % in reference to perfectly dry state

Time of immersion	Wool	Silk	Reworked silk	Ramie	Cotton wool	Viscose rayon
Within 1 hour	19.8	21.0	12.0	20.3	17.8	25.3
1 day	20.1	23.9	19.1	19.7	19.1	35.6
2 days	18.8	25.5	46.6	19.2	19.5	41.7
3 „	——	25.1	52.4	21.1	18.0	46.7
4 „	20.2	25.5	56.9	——	——	50.3
5 „	——	——	56.2	21.5	18.0	51.1
6 „	19.7	25.3	56.2	——	——	50.7

As seen in Table VIII, the lateral swellings in water of wool, silk, ramie and cotton wool attain their maximum values immediately after the immersion. On the other hand, the lateral swellings of reworked

silk and viscose rayon increase gradually as the time goes on, and become very great after several days. This fact seems to suggest that the micellar structure of these artificial fibres is looser than that of natural fibres.

Next by assuming that viscose rayon is reduced to hydratecellulose as $2C_{12}H_{19}O_9OH$ and by taking the dimension of its unit cell which is determined by W. T. Astbury and T. C. Marwick[1] as:

$$a=8.14\text{ A. U.},\quad b=10.3\text{ A. U.},\quad c=9.11\text{ A. U.},\quad \beta=62^\circ,$$

the volume of a unit cell is equal to:

$$V=abc\sin\beta=676.7\times10^{-24}\text{c.c.}.$$

Then the theoretical density ρ_0 is equal to:

$$\rho_0=\frac{4\times162\times1.649\times10^{-24}}{676.7\times10^{-24}}=1.574.$$

The value of the density of the hydratecellulose as calculated above is much smaller than 1.614, the value of the net density of viscose rayon measured by the writer in water and in methyl alcohol. The net densities of wool, ramie and cotton wool which were measured in methyl alcohol are respectively greater too than their theoretical value calculated from their crystal structures determined by the X-ray diffraction, as is shown in Table IX.

As to the cause of such discrepancy between the densities obtained from the X-ray data and from the measurement in methyl alcohol, the presence of some impurities is of course conceivable. But at the same time reexamination of the crystal structures of such fibres seems to be also desirable.

Table IX

	a	b	c	β	Theoretical density	Observed density in methyl alcohol
Wool[2] (Residue)	3.38	4.65	9.8	——	1.231	1.410
Cellulose[3]	8.22	10.33	7.84	84°	1.609	1.627 (ramie)
	8.3	10.3	7.9	84°	1.571	1.641 (cotton)
Viscose rayon[4]	8.14	10.3	9.14	62°	1.574	1.614

1. W. T. Astbury & T. C. Marwick: Nature, **127**, 12 (1931).
2. W. T. Astbury & H. J. Woods: Phil. Trans. Roy. Soc. A **232**, 333 (1933).
3. U. Yoshida & C. Park: These Memoirs, **17**, 443 (1934);
K. H. Meyer & H. Mark: Ber. D. chem. Gesells., **61**, 593 (1928);
„ „ Z. S. physik. Chem., 2B, 115 (1929).
4. W. T. Astbury & T. C. Marwick: Nature, **127**, 12 (1931).

Summary

The main results obtained from the present experiment are summarized below :

(1) The densities of various fibres measured in methyl alcohol are greater than those measured in water, in the other kinds of alcohols and in liquid paraffin. Therefore the net density of fibrous substances which consist of micellar structure must be measured in methyl alcohol.

(2) The difference of the densities of a fibre measured in various primary normal alcohols and in liquid paraffin reveals to some extent the variation of the widths of its intermicellar spaces.

In conclusion the writer wishes to express his sincere gratitude to Prof. U. Yoshida for invaluable suggestions he has given to the present research.

Industrial Physical Laboratory, Nagoya Commercial College.

(Sept. 17, 1938)

On the Oscillation of Lake Water Generated by Wind Action

By **Toshichiro Takegami**

(Received October 10, 1938)

Abstract

In this paper the writer reports mathematical investigations for the oscillation of lake water produced by wind action. For form of basin he has considered the circle, the concentric circles, the sector and the fan-shape.

The method adopted may be described as follows:

1. The cylindrical co-ordinate is used.
2. It is assumed that the bottom of the lake is smooth.
3. It is assumed that the inertia terms and the horizontal convective terms are negligible.
4. Introducing the differential equation which determines the surface elevation, and is analogous to the differential equation for the oscillation of circular membrane in acoustics, he has solved it under the appropriate conditions. The equation obtained is

$$\frac{\partial^2\zeta}{\partial t^2}=\frac{\partial}{\partial r}\left(c^2\frac{\partial\zeta}{\partial r}\right)+\frac{c^2}{r}\frac{\partial\zeta}{\partial r}+\frac{1}{r^2}\frac{\partial}{\partial\theta}\left(c^2\frac{\partial\zeta}{\partial\theta}\right)-\frac{1}{r}\frac{\partial}{\partial r}(rT_r)-\frac{1}{r}\frac{\partial T_\theta}{\partial\theta}$$

where ζ is the surface elevation from the undisturbed surface, r and θ are the radial and the angular co-ordinate, $c^2=gh$ (h being depth of lake), and T_r and T_θ are respectively the radial and the tangential components of wind action.

Introduction

The oscillation of water in a circular or other geometrically regular basin generated by *the gradient of atmospheric pressure* has been investigated by many authors. Practically the oscillation in a basin is mainly generated by *wind action*, but except in a rectangular basin, no investigation of the osillation of water *generated by wind action* in a basin has been reported. In this paper, assuming that the bottom of a lake is smooth, and that the inertia terms and the horizontal convective terms in the equation of motion may be neglected, we shall introduce the differential equation which determines the oscillations generated by wind action when the form of basin is the circle, the concentric circles, the sector, or the fan-shape, and solve it under the suitable conditions.

The Fundamental Equation

Using the cylindrical co-ordinate the equation of motion, the equation of continuity and the boundary conditions at the surface and the bottom are expressed by

$$\frac{\partial v'_r}{\partial t}+v'_r\frac{\partial v'_r}{\partial r}+\frac{v'_\theta}{r}\frac{\partial v'_r}{\partial \theta}-\frac{v'^2_\theta}{r}+v'_z\frac{\partial v'_r}{\partial z}$$
$$=\nu\left(\frac{\partial^2 v'_r}{\partial z^2}+\frac{\partial^2 v'_r}{\partial r^2}+\frac{1}{r}\frac{\partial v'_r}{\partial r}+\frac{1}{r^2}\frac{\partial^2 v'_r}{\partial \theta^2}-\frac{v'_r}{r^2}-\frac{2}{r^2}\frac{\partial v'_\theta}{\partial \theta}\right)$$
$$-g\frac{\partial \zeta}{\partial r} \qquad \cdots\cdots(1),$$

$$\frac{\partial v'_\theta}{\partial t}+v'_r\frac{\partial v'_\theta}{\partial r}+\frac{v'_\theta}{r}\frac{\partial v'_\theta}{\partial \theta}+\frac{v'_r v'_\theta}{r}+v'_z\frac{\partial v_\theta}{\partial z}$$
$$=\nu\left(\frac{\partial^2 v'_\theta}{\partial z^2}+\frac{\partial^2 v'_\theta}{\partial r^2}+\frac{1}{r}\frac{\partial v'_\theta}{\partial r}+\frac{1}{r^2}\frac{\partial^2 v'_\theta}{\partial \theta^2}-\frac{v'_\theta}{r^2}+\frac{2}{r^2}\frac{\partial v'_r}{\partial \theta}\right)$$
$$-g\frac{\partial \zeta}{r\partial \theta} \qquad \cdots\cdots(2),$$

$$\frac{1}{r}\frac{\partial}{\partial r}(\rho v'_r r)+\frac{1}{r}\frac{\partial}{\partial \theta}(\rho v'_\theta)+\frac{\partial}{\partial z}(\rho v_z)=0 \qquad \cdots\cdots(3),$$

and

$$\left.\begin{aligned}\mu\frac{\partial v'_r}{\partial z}&=T_r \quad \mu\frac{\partial v'_\theta}{\partial z}=T_\theta \quad \text{at } z=0\\ \mu\frac{\partial v'_r}{\partial z}&=0 \quad \mu\frac{\partial v'_\theta}{\partial z}=0 \quad \text{at } z=-h\end{aligned}\right\} \qquad \cdots\cdots(4).$$

Here T_r and T_θ are respectively the radial and the tangential component of wind action, and the other notations have the usual meanings, and the vertical motion is only statically and not explicitly concerned.

If, in (1) and (2), the inertia terms $v'_r\frac{\partial v'_r}{\partial r}$, $v'_r\frac{\partial v'_\theta}{\partial r}$ etc. and the horizontal convective terms $\frac{\partial^2 v'_r}{\partial r^2}$, $\frac{1}{r}\frac{\partial v'_r}{\partial r}$ etc. may be neglected (especially, in the circular or the sectorial basin, the neglect of the terms multiplied by $\frac{1}{r}$ and $\frac{1}{r^2}$ seems quite arbitrary), then (1) and (2) become

$$\frac{\partial v'_r\rho}{\partial t}=\nu\frac{\partial^2 v'_r\rho}{\partial z^2}-g\frac{\partial \zeta\rho}{\partial r} \qquad \cdots\cdots(1'),$$

$$\frac{\partial v'_\theta\rho}{\partial t}=\nu\frac{\partial^2 v'_\theta\rho}{\partial z^2}-g\frac{\partial \zeta\rho}{r\partial \theta} \qquad \cdots\cdots(2').$$

Now integrate (1'), (2') and (3) with respect to z from $-h$ to 0, and take into account (4), then we have

$$\frac{\partial S_r}{\partial t}=rT_r-rgh\frac{\partial\zeta\rho}{\partial r} \qquad \cdots\cdots\cdots\cdots\cdots\cdots(1''),$$

$$\frac{\partial S_\theta}{\partial t}=T_\theta-gh\frac{\partial\zeta\rho}{r\partial\theta} \qquad \cdots\cdots\cdots\cdots\cdots\cdots(2''),$$

$$\frac{\partial S_r}{\partial r}+\frac{\partial S_\theta}{\partial\theta}=-r\rho\frac{\partial\zeta}{\partial t} \qquad \cdots\cdots\cdots\cdots\cdots\cdots(3'),$$

where $S_r=\int_{-h}^{0}\rho r v_r dz$ and $S_\theta=\int_{-h}^{0}\rho v_\theta dz$.

By eliminating S_r and S_θ from $(1'')$, $(2'')$ and $(3')$ we get

$$\frac{\partial^2\zeta}{\partial t^2}=\frac{\partial}{\partial r}\left(c^2\frac{\partial\zeta}{\partial r}\right)+\frac{c^2}{r}\frac{\partial\zeta}{\partial r}+\frac{1}{r^2}\frac{\partial}{\partial\theta}\left(c^2\frac{\partial\zeta}{\partial\theta}\right)-\frac{1}{r}\frac{\partial}{\partial r}(rT_r)-\frac{1}{r}\frac{\partial T_\theta}{\partial\theta} \qquad \cdots\cdots\cdots(5),$$

where $c^2\equiv gh$ and $\zeta\equiv\rho\zeta$. This is the required differential equation in the cylindrical co-ordinate which determines the surface elevation ζ. Thus the solution of this equation, under suitable conditions, will give the rising state of the oscillation of water when the forms of basin are respectively the circle, the concentric circles, the sector and the fan-shape. In the following article we shall give the solutions in a simple case when the wind action is uniform over the whole surface of basin and also the depth h is uniform.

1. Circular basin

As an example, we shall consider a simple case in which a uniform wind, its direction being x positive as seen in Fig. 1., suddenly blows over the surface of a circular basin (its radius being a). Now in order to solve (5) under the following initial and boundary conditions, i. e.,

Fig. 1.

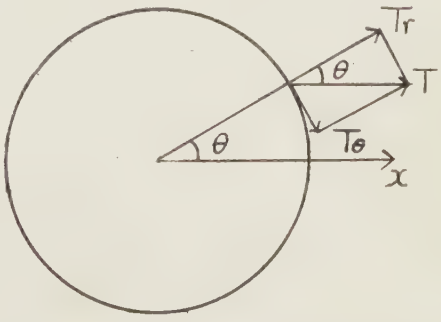

$$\zeta=0,\ \frac{\partial\zeta}{\partial t}=0 \quad \text{when } t=0,$$

$$c^2\frac{\partial\zeta}{\partial r}=T_r=T\cos\theta \quad \text{at } r=a,$$

we shall separate ζ into a stationary part ζ_1 and a varying part $-\zeta_2$ which satisfy $\zeta=\zeta_1-\zeta_2$ and respectively the following two sets of equations and conditions (A) and (B)

$$\text{(A)}\quad \begin{cases} c^2\left\{r^2\dfrac{\partial^2\zeta_1}{\partial r^2}+r\dfrac{\partial\zeta_1}{\partial r}+\dfrac{\partial^2\zeta_1}{\partial\theta^2}\right\}=r\dfrac{\partial}{\partial r}(rT_r)-r\dfrac{\partial T_\theta}{\partial\theta} \\ \qquad\qquad =r\dfrac{\partial}{\partial r}(rT\cos\theta)-r\dfrac{\partial}{\partial\theta}(T\sin\theta)=0, \\ c^2\dfrac{\partial\zeta_1}{\partial r}=T\cos\theta \qquad \text{at } r=a, \\ \zeta_1 \text{ is finite} \qquad \text{at } r=0, \end{cases}$$

$$\text{(B)}\quad \begin{cases} \dfrac{\partial^2\zeta_2}{\partial t^2}=c^2\left\{\dfrac{\partial^2\zeta_2}{\partial r^2}+\dfrac{1}{r}\dfrac{\partial\zeta_2}{\partial r}+\dfrac{1}{r^2}\dfrac{\partial^2\zeta_2}{\partial\theta^2}\right\}, \\ \zeta_2=\zeta_1 \text{ and } \dfrac{\partial\zeta_2}{\partial t}=0 \quad \text{when } t=0, \\ c^2\dfrac{\partial\zeta_2}{\partial r}=0 \qquad \text{at } r=a, \\ \zeta_2 \text{ is finite} \qquad \text{at } r=0. \end{cases}$$

The general solution of (A) is

$$\zeta_1=\left(Ar+\frac{B}{r}\right)\cos\theta+C,$$

and the integration constant A, B and C in the right can be determined from the boundary conditions and the invariableness of water quantity in the basin $\left(\int_0^{2\pi}\int_0^a\zeta_1 r\,dr\,d\theta=0\right)$. Thus we have

$$\zeta_1=\frac{T}{c^2}r\cos\theta.$$

And the solution of (B), which satisfies the conditions, is

$$\zeta_2=\sum_{s=1}^{\infty}\sum_{n=0}^{\infty}\left\{A_{ns}\cos n\theta+B_{ns}\sin n\theta\right\}J_n\left(\lambda_{ns}\frac{r}{a}\right)\cos\left(\lambda_{ns}\frac{ct}{a}\right)$$

where J_n (n being a positive integer) is the Bessel function of the first kind, λ_{ns} are the roots of $J_n'(\lambda)=0$ which has the infinite number of real roots, and

$$A_{ns}=\frac{1}{\pi a^2}\frac{\varepsilon_n\lambda_{ns}^2}{(\lambda_{ns}^2-n^2)J_n^2(\lambda_{ns})}\int_0^a\int_0^{2\pi}\zeta_1(a,\varphi)J_n\left(\lambda_{ns}\frac{a}{a}\right)\cos n\varphi a\,da\,d\varphi,$$

$$B_{ns}=\frac{1}{\pi a^2}\frac{\varepsilon_n\lambda_{ns}^2}{(\lambda_{ns}^2-n^2)J_n^2(\lambda_{ns})}\int_0^a\int_0^{2\pi}\zeta_1(a,\varphi)J_n\left(\lambda_{ns}\frac{a}{a}\right)\sin n\varphi a\,da\,d\varphi,$$

$$\varepsilon_0=1,\ \varepsilon_1=\varepsilon_2=\cdots\cdots\cdots\cdots=2.$$

Since, in our case, T is independent of t and x, A_{ns} and B_{ns} reduce to very simple forms, i. e.,

$$A_{ns}=0 \quad \text{for} \quad n\neq 1, \quad B_{ns}=0 \quad \text{for all values of } n,$$

Table V

Values of $\frac{V_2''}{V_1}$

	Wool	Silk (Fibroin)	Reworked silk	Ramie	Cotton wool	Viscose rayon
Water	0.513	——	——	0.523	0.506	0.981
Methyl alcohol	0.170	0.220	0.171	0.171	0.190	0.667
Ethyl alcohol	0.078	0.248	0.167	0.207	0.176	0.598
n. Propyl alcohol	0.088	0.220	0.119	0.281	0.168	0.083
n. Butyl alcohol	0.126	0.209	0.106	0.207	0.158	0.151
n. Amyl alcohol	0.067	0.195	0.108	0.189	0.102	0.142
Liquid paraffin	0.067	0.088	0.084	0.072	0.053	0.060

As was reported in a previous paper,[1] silk fibroin swells in water both in inter- and intramiceller manner. But in the alcohols and in liquid paraffin intermicellar swelling only occurs with silk; and with all other fibres examined in the present experiment no intramicellar swelling was detected with any kind of liquid examined. So in the following all calculations made are assumed to apply to intermicellar swelling, omitting the exceptional case of silk and reproduced silk in water.

Now let us denote by

D : the net density of a fibrous material

V_1 : the net volume of a fibrous material

M : the net mass of a fibrous material

v : the volume of intermicellar space of a fibrous material in perfectly dried state

V_2'' : the volume of intermicellar space of a fibrous material when it is swollen entirely in a certain liquid

v' : the volume of the intermicellar space into which the liquid molecules cannot intrude when fully swollen in a certain liquid

d : the apparent density of a fibre measured in a liquid

s : the increased volume percentage of a fibre when swollen in a certain liquid as compared with perfectly dried state.

Though it is conceivable that there are some very tiny intermicellar spaces of a fibre into which even the molecules of methyl alcohol cannot intrude, in the following we take approximately the density of a fibre measured in methyl alcohol as D, i. e. the net density of the

1. Y. Matsunaga: *loc. cit.*

fibre. Next let d_p be the density of a fibre measured in liquid paraffin, and if we assume roughly that the liquid paraffin molecules cannot intrude into the intermicellar space of a fibre entirely, as the density of a fibre is minimum in liquid paraffin so far as the present experiment is concerned, then

$$\frac{M}{V_1}=D, \text{ or } M=DV_1, \qquad (1)$$

$$\frac{M}{V_1+v}=\frac{DV_1}{V_1+v}=\frac{D}{1+\frac{v}{V_1}}=d_p. \qquad (2)$$

By putting the values of D and d_p as tabulated in Table I in the equation (2), we get the numerical values of $\frac{v}{V_1}$ for various fibres.

Now, from the density of a fibre measured in a liquid, we have the following equation:

$$\frac{M}{V_1+v'}=\frac{DV_1}{V_1+v'}=\frac{D}{1+\frac{v'}{V_1}}=d, \qquad (3)$$

and we obtained the numerical values of $\frac{v'}{V_1}$ as given in Table VI.

On the other hand, from the increase of volume of a fibre by swelling we have the relation:

$$\frac{V_1+V_2''-(V_1+v)}{V_1+v}=\frac{1+\frac{V_2''}{V_1}-\left(1+\frac{v}{V_1}\right)}{1+\frac{v}{V_1}}=s. \qquad (4)$$

Table VI

Values of $\frac{v'}{V_1}$

	Wool	Silk (Fibroin)	Reworked silk	Ramie	Cotton wool	Viscose rayon
Water	0.008	——	——	0.009	0.023	0.000
Methyl alcohol	0.000	0.000	0.000	0.000	0.000	0.000
Ethyl alcohol	0.003	0.027	0.022	0.022	0.003	0.022
n. Propyl alcohol	0.027	0.072	0.058	0.024	0.028	0.022
n. Butyl alcohol	0.031	0.073	0.054	0.028	0.028	0.032
n. Amyl alcohol	0.032	0.072	0.053	0.030	0.025	0.041
Liquid paraffin	0.067	0.088	0.084	0.072	0.053	0.060

and
$$A_{1s}=\frac{2T}{c^2}\frac{a}{\lambda_{1s}(\lambda_{1s}^2-1^2)J_1^2(\lambda_{1s})}\int_0^{\lambda_{1s}}\beta^2 J_1(\beta)d\beta$$
$$-\frac{2Ta}{c^2}\frac{1}{(\lambda_{1s}^2-1^2)J_1(\lambda_{1s})},\quad\left(\beta\text{ being }\frac{\lambda_{1s}a}{a}\right),$$

therefore
$$\zeta_2=\frac{2Ta}{c^2}\cos\theta\sum_{s=1}^{\infty}\frac{1}{(\lambda_{1s}^2-1^2)J_1(\lambda_{1s})}J_1\left(\lambda_{1s}\frac{r}{a}\right)\cos\left(\lambda_{1s}\frac{ct}{a}\right).$$

And our required solution is

Fig. 2. (a)

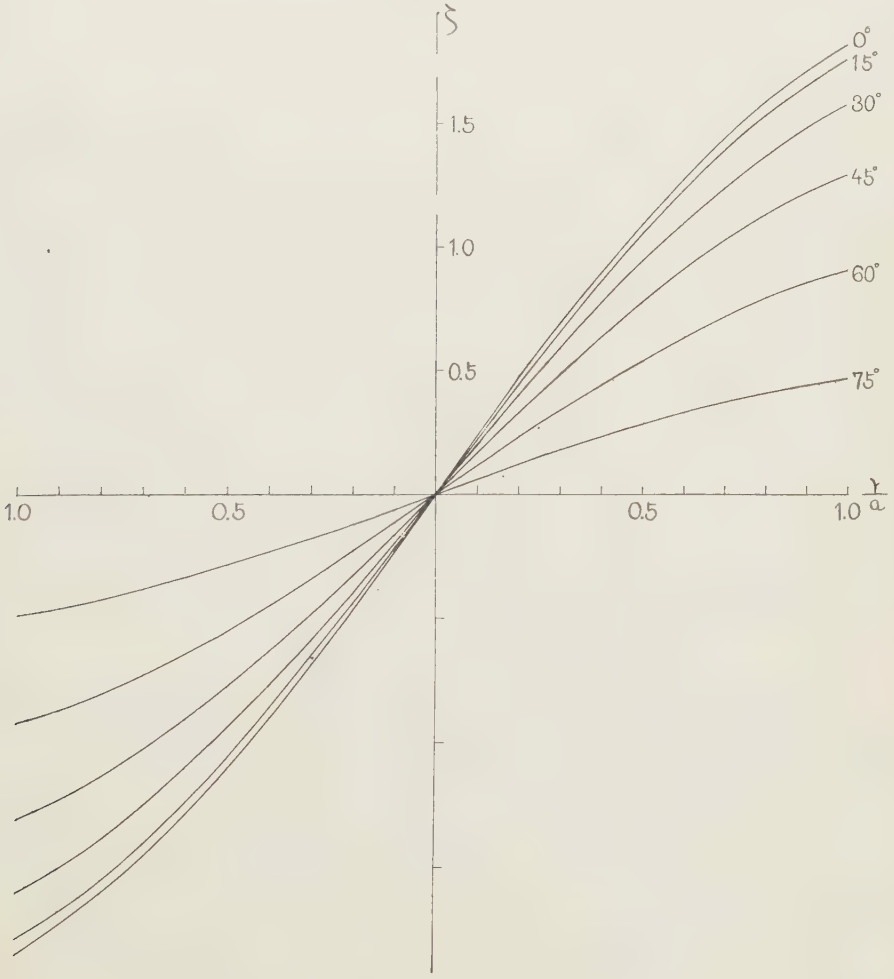

$$\zeta=\frac{T}{\rho gh}a\cos\theta\left\{\frac{r}{a}-2\sum_{s=1}^{\infty}\frac{1}{(\lambda_{1s}^2-1^2)J_1(\lambda_{1s})}J_1\left(\lambda_{1s}\frac{r}{a}\right)\cos\left(\lambda_{1s}\frac{ct}{a}\right)\right\},$$

or if T varies with the time, from Nomitsu's extension[1] of the Duhamel theorem, we get

$$\zeta=\frac{2c}{\rho gh}\sum_{s=1}^{\infty}\frac{\lambda_{1s}}{(\lambda_{1s}^2-1^2)J_1(\lambda_{1s})}\cos\theta J_1\left(\lambda_{1s}\frac{r}{a}\right)\int_0^t T(\tau)\sin\frac{\lambda_{1s}c}{a}(t-\tau)d\tau.$$

After carrying out the numerical calculations, we get Figs. 2 (a) and (b) which give respectively the sum of ζ_1 and the first harmonic

Fig. 2. (b)

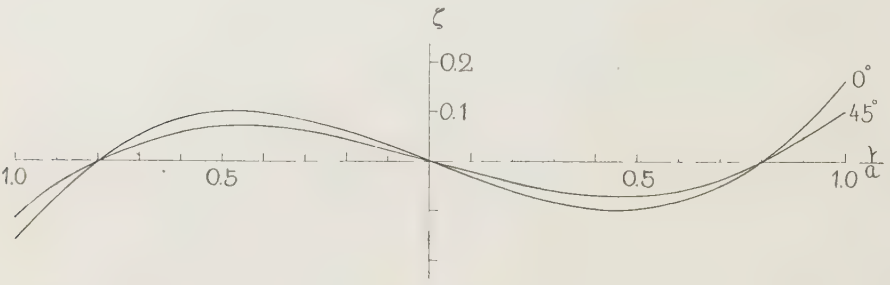

of the elevation $-\zeta_2$, at two epochs $\frac{\pi}{1.841}\frac{a}{c}$ and $\frac{2\pi}{1.841}\frac{a}{c}$, in the seven vertical sections which pass the centre of basin and have an angular interval of 15° to each other, where 1.841 is a root λ_{11} of $J_1'(\lambda)=0$ and $\frac{Ta}{\rho gh}$ is taken as the unit of ζ. But since the elevations in the other half sections are symmetrical, in respect to the line $\theta=0$, to these figures, they need not be given.

2. Concentric Circular Basin

In this case the sets of equation and conditions corresponding to (A) and (B) in the previous article are

$$(A')\begin{cases} r^2\frac{\partial^2\zeta_1}{\partial r^2}+r\frac{\partial\zeta_1}{\partial r}+\frac{\partial^2\zeta_1}{\partial\theta^2}=0 \\ c^2\frac{\partial\zeta_1}{\partial r}=T\cos\theta \quad \text{at} \quad r=a \quad \text{and} \quad r=b, \end{cases}$$

1. Proc. Imp. Acad. Tokyo, **11**, 359 (1935).

$$(B')\begin{cases}\dfrac{\partial^2\zeta_2}{\partial t^2}=c^2\left\{\dfrac{\partial^2\zeta_2}{\partial r^2}+\dfrac{1}{r}\dfrac{\partial\zeta_2}{\partial r}+\dfrac{1}{r^2}\dfrac{\partial^2\zeta_2}{\partial\theta^2}\right\}\\ \zeta_2=\zeta_1 \text{ and } \dfrac{\partial\zeta_2}{\partial t}=0 \qquad \text{when } t=0\\ c^2\dfrac{\partial\zeta_2}{\partial r}=0 \qquad \text{at } r=a \text{ and } r=b,\end{cases}$$

where a and b are respectively the inner and the outer radius of the concentric circle.

The solution of (A′) is obviously

$$\zeta_1=\frac{T}{c^2}r\cos\theta.$$

And the solution of (B′), after some calculation, is represented by

$$\zeta_2=\sum_{s=1}^{\infty}\sum_{n=0}^{\infty}\left\{A_{ns}\cos n\theta+B_{ns}\sin n\theta\right\}K_n\left(\lambda_{ns}\frac{r}{a}\right)\cos\left(\lambda_{ns}\frac{ct}{a}\right),$$

where $$K_n\left(\lambda_{ns}\frac{r}{a}\right)=\frac{J_n\left(\lambda_{ns}\frac{r}{a}\right)}{J_n'(\lambda_{ns})}-\frac{Y_n\left(\lambda_{ns}\frac{r}{a}\right)}{Y_n'(\lambda_{ns})},$$

Y_n (n being a positive integer) is the Bessel function of the second kind, λ_{ns}'s are the roots of $J_n'\left(\lambda\frac{b}{a}\right)Y_n'(\lambda)-J_n'(\lambda)Y_n'\left(\lambda\frac{b}{a}\right)=0$,

$$A_{ns}=\frac{1}{\pi a^2}\cdot\frac{\varepsilon_n\lambda_{ns}^2}{(\lambda_{ns}^2-n^2)K_n^2(\lambda_{ns})-\left(\lambda_{ns}^2\frac{b^2}{a^2}-n^2\right)K_n^2\left(\lambda_{ns}\frac{b}{a}\right)}$$
$$\times\int_b^a\int_0^{2\pi}\zeta_1(\alpha,\varphi)K_n\left(\lambda_{ns}\frac{\alpha}{a}\right)\cos n\varphi\,\alpha\,d\alpha\,d\varphi,$$

$$B_{ns}=\frac{1}{\pi a^2}\cdot\frac{\varepsilon_n\lambda_{ns}^2}{(\lambda_{ns}^2-n^2)K_n^2(\lambda_{ns})-\left(\lambda_{ns}^2\frac{b^2}{a^2}-n^2\right)K_n^2\left(\lambda_{ns}\frac{b}{a}\right)}$$
$$\times\int_b^a\int_0^{2\pi}\zeta_1(\alpha,\varphi)K_n\left(\lambda_{ns}\frac{\alpha}{a}\right)\sin n\varphi\,\alpha\,d\alpha\,d\varphi,$$

$$\varepsilon_0=1,\ \varepsilon_1=\varepsilon_2=\ldots\ldots\ldots\ldots=2.$$

But since in our case $\zeta_1=\frac{T}{c^2}\alpha\cos\varphi$,

$$A_{ns}=0 \text{ for } n\neq 1 \text{ and } B_{ns}=0 \text{ for all values of } n,$$

and by using the recurring formulae of Bessel function, A_{1s} may be reduced to the following simple form:

$$A_{1s}=\frac{1}{a^2}\frac{2\lambda_{1s}}{(\lambda_{1s}^2-1^2)K_1^2(\lambda_{1s})-\left(\lambda_{1s}^2\frac{b^2}{a^2}-1^2\right)K_1^2\left(\lambda_{1s}\frac{b}{a}\right)}\int_b^a\frac{T}{c^2}\alpha^2K_1\left(\lambda_{1s}\frac{\alpha}{a}\right)d\alpha$$

$$= \frac{Ta}{c^2} \frac{2\left\{K_1(\lambda_{1s}) - \frac{b}{a}K_1\left(\lambda_{1s}\frac{b}{a}\right)\right\}}{(\lambda_{1s}^2 - 1^2)K_1^2(\lambda_{1s}) - \left(\lambda_{1s}^2\frac{b^2}{a^2} - 1^2\right)K_1^2\left(\lambda_{1s}\frac{b}{a}\right)},$$

therefore we have

$$\zeta_2 = \sum_{s=1}^{\infty} A_{1s}\cos\theta K_1\left(\lambda_{1s}\frac{r}{a}\right)\cos\left(\lambda_{1s}\frac{ct}{a}\right).$$

Thus our required solution is

$$\zeta = \frac{Ta}{\rho gh}\cos\theta\left\{\frac{r}{a} - 2\sum_{s=1}^{\infty}\frac{K_1(\lambda_{1s}) - \frac{b}{a}K_1\left(\lambda_{1s}\frac{b}{a}\right)}{(\lambda_{1s}^2 - 1^2)K_1^2(\lambda_{1s}) - \left(\lambda_{1s}^2\frac{b^2}{a^2} - 1^2\right)K_1^2\left(\lambda_{1s}\frac{b}{a}\right)}\right.$$
$$\left.\times K_1\left(\lambda_{1s}\frac{r}{a}\right)\cos\left(\lambda_{1s}\frac{ct}{a}\right)\right\},$$

or if T varies with the time, from Nomitsu's extension of the Duhamel theorem, we have

$$\zeta = \frac{2c}{\rho gh}\cos\theta\sum_{s=1}^{\infty}\frac{\left\{K_1(\lambda_{1s}) - \frac{b}{a}K_1\left(\lambda_{1s}\frac{b}{a}\right)\right\}\lambda_{1s}}{(\lambda_{1s}^2 - 1^2)K_1^2(\lambda_{1s}) - \left(\lambda_{1s}^2\frac{b^2}{a^2} - 1^2\right)K_1^2\left(\lambda_{1s}\frac{b}{a}\right)}$$
$$\times K_1\left(\lambda_{1s}\frac{r}{a}\right)\int_0^t T(\tau)\sin\frac{\lambda_{1s}c}{a}(t-\tau)d\tau.$$

Fig. 3. (a)

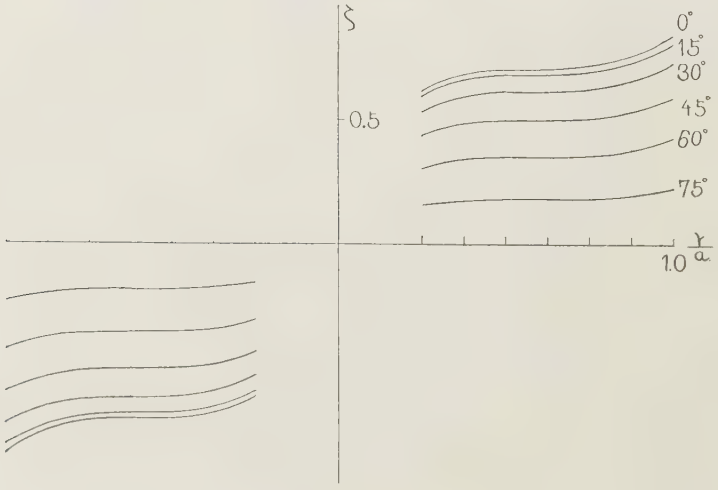

As an example, we consider a case of $\frac{b}{a}=3$, and after carrying out the numerical calculations, we get Figs. 3 (a) and (b) which give respectively the sum of ζ_1 and the first harmonic of the elevation $-\zeta_2$, at two epochs $\frac{\pi}{5.205}\frac{a}{c}$ and $\frac{2\pi}{5.205}\frac{a}{c}$, in the seven vertical sections which pass the centre of the basin and have an angular interval of 15° to each other, where 5.205 is a root λ_{11} of $J_1'\left(\lambda\frac{b}{a}\right)Y_1'(\lambda)-J_1'(\lambda)\times Y_1'\left(\lambda\frac{b}{a}\right)=0$, and $\frac{Ta}{\rho gh}$ is taken as the unit of ζ. But since the

Fig. 3. (b)

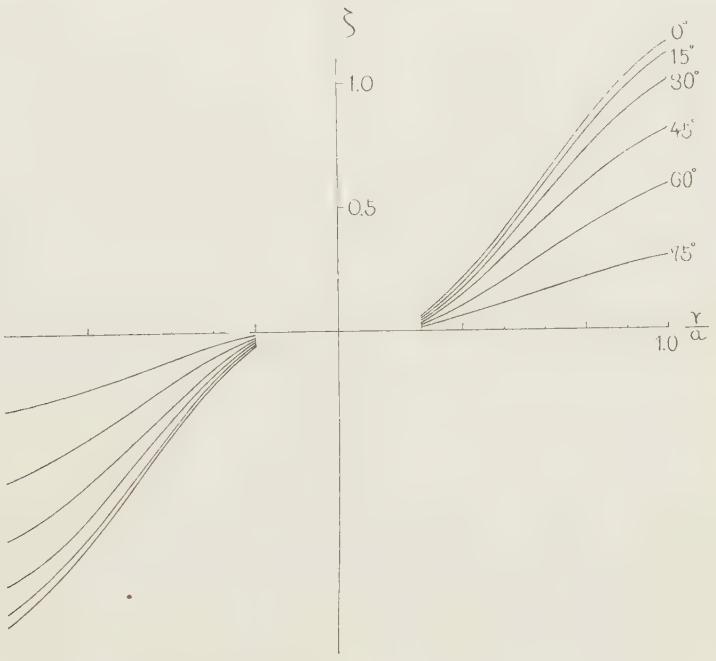

elevations in the other half sections are in symmetry, in respect to the line $\theta=0$, to these figures, they need not be given.

3. Sectorial Basin

Consider the sectorial basin surrounded by two lines $\theta=0$, $\theta=\alpha$ and an arc (its radius being a), and the direction of wind making an angle θ_0 with the line $\theta=0$. Then the sets of equations and conditions are

$$(A'')\begin{cases} r^2\dfrac{\partial^2\zeta_1}{\partial r^2}+r\dfrac{\partial\zeta_1}{\partial r}+\dfrac{\partial^2\zeta_1}{\partial\theta^2}=0 \\ c^2\dfrac{\partial\zeta_1}{\partial r}=T\cos(\theta-\theta_0) & \text{at } r=a \\ \zeta_1 \text{ is finite} & \text{at } r=0 \\ c^2\dfrac{\partial\zeta_1}{r\partial\theta}=T\sin\theta_0 & \text{at } \theta=0 \\ c^2\dfrac{\partial\zeta_1}{r\partial\theta}=-T\sin(\alpha-\theta_0) & \text{at } \theta=\alpha, \end{cases}$$

$$(B'')\begin{cases} \dfrac{\partial^2\zeta_2}{\partial t^2}=c^2\left\{\dfrac{\partial^2\zeta_2}{\partial r^2}+\dfrac{1}{r}\dfrac{\partial\zeta_2}{\partial r}+\dfrac{1}{r^2}\dfrac{\partial^2\zeta_2}{\partial\theta^2}\right\} \\ \zeta_2=\zeta_1 \text{ and } \dfrac{\partial\zeta_2}{\partial t}=0 & \text{when } t=0 \\ c^2\dfrac{\partial\zeta_2}{\partial r}=0 & \text{at } r=a \\ \zeta_2 \text{ is finite} & \text{at } r=0 \\ c^2\dfrac{\partial\zeta_2}{r\partial\theta}=0 & \text{at } \theta=0 \text{ and } \theta=\alpha. \end{cases}$$

The solution of (A'') is

$$\zeta_1=\frac{Ta}{c^2}\left\{\frac{r}{a}\cos(\theta-\theta_0)-\frac{2}{3}\frac{\sin(\alpha-\theta_0)+\sin\theta_0}{\alpha}\right\},$$

and the solution of (B'') is

$$\zeta_2=\sum_{s=1}^{\infty}\sum_{m=1}^{\infty}A_{ms}\cos n\theta J_n\left(\lambda_{ms}\frac{r}{a}\right)\cos\left(\lambda_{ms}\frac{ct}{a}\right),$$

where $n\equiv\dfrac{m\pi}{\alpha}$, λ_{ms}'s are the roots of $J_n'(\lambda)=0$ and

$$A_{ms}=\frac{2}{a\alpha^2}\sum_{s=1}^{\infty}\sum_{m=1}^{\infty}\frac{\lambda_{ms}^2}{(\lambda_{ms}^2-n^2)J_n^2(\lambda_{ms})}\int_0^a\int_0^{\alpha}\zeta_1(\beta,\varphi)J_n\left(\lambda_{ms}\frac{\beta}{\alpha}\right)\cos n\varphi_1\beta d_1\beta d\varphi.$$

Thus the required solution is given by subtracting the above ζ_2 from ζ_1.

As an example, we took up a case where $\theta_0=0$ and $\alpha=\dfrac{2\pi}{3}$, and carried out the numerical calculation for a term of $m=1$ and $s=1$. Then this term becomes

$$[\zeta_2]_{m=1,\ s=1}=0.660\frac{Ta}{\rho gh}\frac{J_{\frac{3}{2}}\left(\lambda_1\dfrac{r}{a}\right)\cos\dfrac{3}{2}\theta\cos\left(\lambda_1\dfrac{ct}{a}\right)}{\left(\lambda_1^2-\left(\dfrac{3}{2}\right)^2\right)J_{\frac{3}{2}}^2(\lambda_1)}\left\{\frac{5}{4\lambda_1}\int_0^{\lambda_1}\sqrt{\frac{2}{\pi\gamma}}\cos\gamma d\gamma\right.$$

$$-\frac{3\sqrt{3}}{4\pi}\int_0^{\lambda_1}\sqrt{\frac{2}{\pi\gamma}}\sin\gamma d\gamma-\frac{5}{2}\frac{\cos\lambda_1}{\sqrt{\lambda_1}}+\frac{\sqrt{3}-2\pi}{2\pi}\sqrt{\lambda_1}\sin\lambda_1\Bigg\},$$

$\gamma\equiv\lambda_1\frac{\beta}{\alpha}$ and $\lambda_1=2.463$ is a root of $J_{\frac{3}{2}}'(\lambda)=0$.

And the definite integrals $\int_0^{\lambda_1}\sqrt{\frac{2}{\pi\gamma}}\cos\gamma d\gamma$ and $\int_0^{\lambda_1}\sqrt{\frac{2}{\pi\gamma}}\sin\gamma d\gamma$ in the above expression are respectively reduced to a well known rapidly convergent series

Fig. 4. (a)

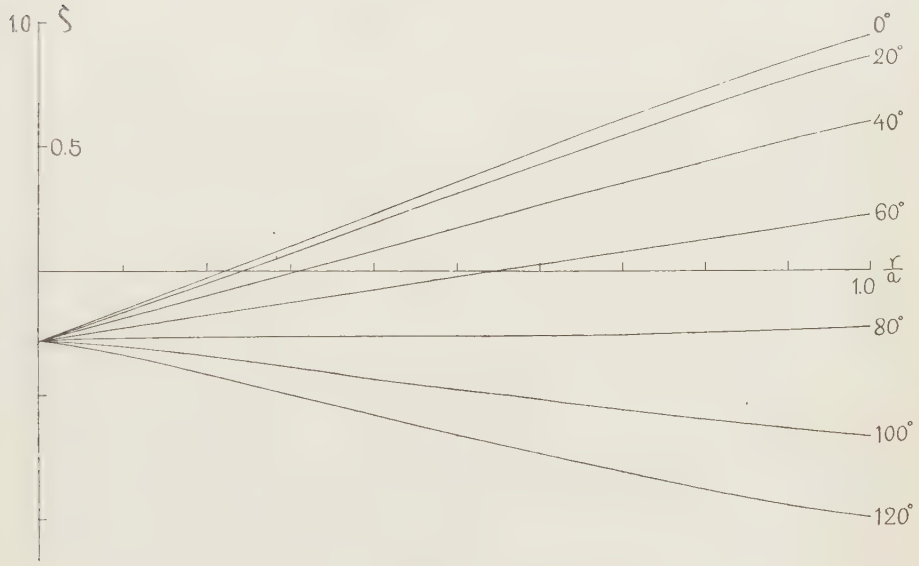

Fig. 4. (b)

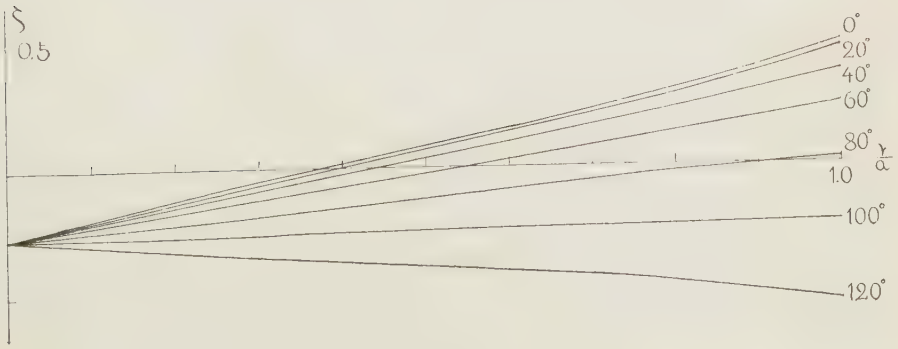

$$2\left\{J_{\frac{1}{2}}(\lambda_1)+J_{\frac{5}{2}}(\lambda_1)+J_{\frac{9}{2}}(\lambda_1)+\cdots\cdots\right\} \text{ and } 2\left\{J_{\frac{3}{2}}(\lambda_1)+J_{\frac{7}{2}}(\lambda_1)+J_{\frac{11}{2}}(\lambda_1)+\cdots\cdots\right\}.$$

Calculating $\zeta_1-[\zeta_2]_{\substack{s=1\\m=1}}$, at two epochs $\frac{\pi}{2.463}\frac{a}{c}$ and $\frac{2\pi}{2.463}\frac{a}{c}$, by these formulae, Figs. 4 (a) and (b) are obtained.

When the wind action T varies with the time, the solution may be obtained by using, also, Nomitsu's extension of the Duhamel theorem, i. e.,

$$\zeta=\frac{2c}{\alpha a^3}\sum_{s=1}^{\infty}\sum_{m=1}^{\infty}\frac{\lambda_{ns}^3 J_n\left(\lambda_{ns}\frac{r}{a}\right)\cos n\theta}{(\lambda_{ns}^2-n^2)J_n^2(\lambda_{ns})}\int_0^a\int_0^\alpha\int_0^t\zeta_1(\tau,\beta,\varphi)J_n\left(\lambda_{ns}\frac{\beta}{a}\right)$$
$$\times\cos n\varphi\sin\frac{\lambda_{ns}c}{a}(t-\tau)\beta d\beta d\varphi d\tau.$$

4. Fan-shaped Basin

In this case it is sufficient that the conditions—ζ_1 and ζ_2 are finite at $r=0$ in (A″) and (B″)—are respectively replaced with the conditions $c^2\frac{\partial\zeta_1}{\partial r}=T\cos(\theta-\theta_0)$ at $r=b$ and $c^2\frac{\partial\zeta_2}{\partial r}=0$ at $r=b$.

Then
$$\zeta_1=\frac{Ta}{c^2}\left\{\frac{r}{a}\cos(\theta-\theta_0)-\frac{2}{3}\frac{a^3-b^3}{a(a^2-b^2)}\frac{\sin(\alpha-\theta_0)+\sin\theta_0}{\alpha}\right\}$$

and
$$\zeta_2=\sum_{s=1}^{\infty}\sum_{m=1}^{\infty}A_{ns}\cos n\theta L_n\left(\lambda_{ns}\frac{r}{a}\right)\cos\left(\lambda_{ns}\frac{ct}{a}\right),$$

where λ_{ns}'s are the roots of $J_n'(\lambda)J_{-n}'\left(\lambda\frac{b}{a}\right)-J_n'\left(\lambda\frac{b}{a}\right)J_{-n}'(\lambda)=0$, n is $\frac{m\pi}{\alpha}$,

$$A_{ns}=\frac{2}{\alpha a^2}\frac{\lambda_{ns}^2}{(\lambda_{ns}^2-n^2)L_n^2(\lambda_{ns})-\left(\lambda_{ns}^2\frac{b^2}{a^2}-n^2\right)L_n^2\left(\lambda_{ns}\frac{b}{a}\right)}$$
$$\times\int_b^a\int_0^\alpha\zeta_1(\beta,\varphi)L_n\left(\lambda_{ns}\frac{r}{a}\right)\cos n\varphi\,\beta d\beta\,d\varphi,$$

and
$$L_n=\frac{J_n\left(\lambda\frac{r}{a}\right)}{J_n'(\lambda)}-\frac{J_{-n}\left(\lambda\frac{r}{a}\right)}{J_{-n}'(\lambda)}.$$

Since the numerical calculations of these formulae are very tedious, we have given only the formal solution without the figures corresponding to those given in the preceding cases.

Now it must be noted that, if the equations of motion and of continuity are expressed by another curvilinear co-ordinate such as

the elliptic cylinder or the parabolic cylinder etc., we may give, in a form similar to that of the present paper, the differential equation for ζ in another geometrically regular basin. Especially since, when the basin is elliptic, the solution of the differential equation may be applied to the generating stage of oscillation in Osaka bay, it will be of great interest. But since it is very tedious and difficult to obtain the solution, we shall leave the matter to expert mathematicians.

In conclusion the writer wishes to express his sincere thanks to Prof. T. Nomitsu for his kind advice and encouragement during the study.

INDEX OF AUTHORS TO VOLUME XXI

PAGE

Kano, H.—(See **Tanaka, K.** and **Kano, H.**) 1

Kurihara, M.—Strahlungstheoretische Untersuchungen über die Stellargashülle in Bewegung 89

Matsunaga, Y.—On the Densities of Various Fibres and the Widths of the Intermicellar Spaces 217

Miyamoto, S.—On the Balmer Emission of the Planetary Nebulae 173

Nakae, T.—Eine Anwendung der Quaternionen zur Kugelgeometrie 5

Namba, M.—An Investigation of Earth Currents on the Volcano Aso, Part I. The Potential Difference of the Upward Earth-current flowing toward the top of a Volcano 203

Namekawa, T. and **Takahasi, T.**—A Theoretical Note on the Diurnal Variation of Wind-Vector due to the Variation of Eddy Viscosity 31

Satô, T.—On the Proof of Carleman's Extension Theorem of Liouville Theorem . . 47

Shirai, T.—On the Condition of the Set which might be a Derived Set 51

Sugihara, M.—Change of the Elastic Limit of an Aluminium Rod by Annealing . . 145

Sugihara, M.—Elastic Property of an Aluminium Rod and its Crystal Grains 163

Takahasi, T.—(See **Namekawa, T.** and **Takahasi, T.**) 31

Takegami, T.—A Study of the Effect of a Travelling Atmospheric Disturbance upon the Sea-Surface 55

Takegami, T.—On the Oscillation of Lake Water Generated by Wind Action 231

Tanaka, K. and **Kano, H.**—The Oxidation of Aluminium Foils 1

Tanaka, K.—Temperature Variation of Electron Diffraction Patterns of Some Organic Films 85

Tanaka, K.—Examination of Thin Rubber Films by Electron Diffraction 169

Terada, T.—Effect of High Frequency Oscillation on the Photo-electric Current . . . 39

Yamamori, S. and **Yoshimoto, S.**—On the Crystalline Configurations of Electrolytic Lead deposited from Nitrate Solutions 75

Yoshimoto, S.—(See **Yamamori, S.** and **Yoshimoto, S.**) 75

INDEX OF SUBJECTS TO VOLUME XXI

PAGE

Aluminium Foils, The Oxidation of, (*Tanaka* and *Kano*) 1
Aluminium Rod by Annealing, Change of the Elastic Limit of an, (*Sugihara*) . . . 145
Aluminium Rod and its Crystal Grains, Elastic Property of an, (*Sugihara*) 163
Balmer Emission of the Planetary Nebulae, On the, (*Miyamoto*) 173
Carleman's Extension Theorem of Liouville Theorem, On the Proof of, (*Satô*) . . . 47
Densities of Various Fibres and the Widths of the Intermicellar Spaces, On the, (*Matsunaga*) 217
Diurnal Variation of Wind-Vector due to the Variation of Eddy Viscosity, A Theoretical Note on the, (*Namekawa* and *Takahasi*) 31
Earth Currents on the Volcano Aso, Part I. The Potential Difference of the Upward Earth-current flowing toward the top of a Volcano, An Investigation of, (*Namba*) 203
Electrolytic Lead deposited from Nitrate Solutions, On the Crystalline Configurations of, (*Yamamori* and *Yoshimoto*) 75
Electron Diffraction Patterns of Some Organic Films, Temperature Variation of, (*Tanaka*) 85
Oscillation of Lake Water Generated by Wind Action, On the, (*Takegami*) 231
Photo-electric Current, Effect of High Frequency Oscillation on the, (*Terada*) 39
Quaternionen zur Kugelgeometrie, Eine Anwendung der, (*Nakae*) 5
Rubber Films by Electron Diffraction, Examination of Thin, (*Tanaka*) 169
Set which might be a Derived Set, On the Condition of the, (*Shirai*) 51
Stellargashülle in Bewegung, Strahlungstheoretische Untersuchungen über die, (*Kurihara*) 89
Travelling Atmospheric Disturbance upon the Sea-Surface, A Study of the Effect of a, (*Takegami*) 55